Calculation of Irregular Wave Reflection from Perforated-Wall Caisson Breakwaters Using a Regular Wave Model

규칙파 모델을 이용한 유공 케이슨 방파제로부터의 불규칙파 반사율 산정

지도교수 서 경 덕

이 논문을 공학석사 학위논문으로 제출함

2001년 10월

서울대학교 대학원

지구환경시스템공학부

손 상 영

손 상 영의 공학석사 학위논문으로 인준함

2001년 12월

위 원 장 _____

부위원장 _____

위 원 _____

ABSTRACT

Analytical models that can predict the reflection of regular or irregular waves from a perforated-wall caisson breakwater have been developed. Though such irregular wave models as Suh et al. (2001) become available, regular wave models are still in extensive use because of their simplicity. In the present study, using the regular wave model of Fugazza and Natale (1992), we calculated the reflection of irregular waves from a perforated-wall caisson breakwater in several different methods.

First, the regular wave model was re-validated by the hydraulic model tests. Though the model somewhat over-predicted the reflection coefficients at larger values and under-predicted them at smaller values, overall agreement was pretty good between calculation and measurement.

Then, the regular wave model was applied to calculate the irregular wave reflection in the experiments of Suh et al. (2001) and Bennett et al. (1992). In applying the regular wave model to irregular wave reflection, several different methods were used. The results showed that it is the most reasonable to use the regular wave model repeatedly for each frequency component of the irregular wave spectrum with the root-mean-squared wave height for all the frequencies.

Keywords : regular waves, irregular waves, laboratory experiments, wave reflection, perforated-wall caisson breakwaters

TABLE OF CONTENTS

LIST OF FIGURES

LIST OF TABLES

LIST OF SYMBOLS

LATIN

A	Half distance between the centers of two adjacent members of slit wall
a	Half width of a slit
B	Wave chamber width of the perforated-wall caisson
C	Blockage coefficient
C_c	Empirical contraction coefficient
C_l	Energy loss coefficients
C_r	Reflection coefficients
$\overline{C_r}$	Frequency-averaged reflection coefficients
d	Thickness of the perforated-wall
f	Frequency
g	Gravitational acceleration
H	Wave height
H_s	Significant wave height
h	Constant water depth in still water
k	Wave number
L	Wave length
ℓ	Length of the jet following through the perforated wall

$m_{0,i}$	Zeroth moments of the incident wave spectra
$m_{0,r}$	Zeroth moments of the reflected wave spectra
r	Porosity
$S_i(f)$	Incident wave energy spectrum
$S_r(f)$	Reflected wave energy spectrum
T_s	Significant wave period

GREEK

α	Energy loss coefficient
β	Linearized dissipation coefficient
η	Surface elevation
ρ	Fluid density
Φ	Velocity potential
Ω	Fluid domain
ω	Angular frequency

SUPERSCRIPT

c	Calculation
m	Measurement

SUBSCRIPT

i	Incident wave
r	Reflected wave

LIST OF PHOTOS

CHAPTER 1

INTRODUCTION

1.1 Research Backgrounds

A perforated-wall caisson is often used to remedy the drawbacks of a conventional vertical-wall caisson. It has some desirable features that have encouraged its use within harbors. It reduces not only wave reflection but also wave transmission due to overtopping. It also reduces wave force, especially impulsive wave force, acting on the caisson (Takahashi and Shimosako, 1994; Takahashi et al., 1994). Numerous theoretical or experimental studies for the perforated-wall caisson have been performed to investigate its hydraulic and hydrodynamic characteristics.

1.2 Literature Survey

In order to examine the reflection characteristics of a perforated-wall caisson breakwater, hydraulic model tests have been used (Tanimoto et al., 1976; Ijima et al., 1978; Kakuno et al. 1992; Park et al., 1993 among others). Tanimoto et al. (1976) reported hydraulic model experiments for the reflection from a perforated-wall caisson mounted on a rubble foundation of irregular

waves of the Bretschneider-Mitsuyasu spectrum. But their experiments were only for the normally incident waves. Ijima et al. (1978) carried out hydraulic model experiments for obliquely incident waves upon the breakwater. Kakuno et al. (1992) performed hydraulic model experiments for wave reflection from a perforated-wall caisson breakwater installed on a flat bed without a mound. On the other hand, Park et al. (1993) carried out hydraulic model experiments for wave reflection from a partially perforated-wall caisson mounted on a rubble mound.

Efforts have also been made toward developing analytical models for predicting the reflection coefficient (Kondo, 1979; Kakuno et al., 1992; Bennett et al., 1992; Fugazza and Natale, 1992; Suh and Park, 1995). Based upon the linearized shallow water wave theory, Kondo (1979) developed an analytical model for calculating reflection coefficient of a perforated caisson having one or two wave chambers using dividing region method. Kondo showed that for reducing wave reflection the breakwater having two wave chambers is more effective than that having one, only when $B/L > 0.3$, in which B is the chamber width and L is the wave length. He also showed that a perforated caisson gives a lower reflection coefficient when the second porous wall was located at the center between the front porous wall and the rear impervious wall.

Fugazza and Natale (1992) proposed a closed-form solution for wave reflection from a multi-chamber perforated-wall caisson. They showed that the

reflection is minimized when the wave chamber width is about one quarter of the wavelength, i.e., $B/L = 0.25$. And they also proved that the perforated-wall breakwater with a single chamber could give the largest reduction of wave reflection in the range of practical applications.

Kakuno et al. (1992) developed an analytical model for predicting wave reflection from a single-chamber perforated-wall caisson using a modified method of matched asymptotic expansions. They showed that the leading order solutions are accurate enough and could be used to calculate reflection coefficients and the wave action in the vicinity of the breakwater. On the other hand, based on the extended refraction-diffraction equation proposed by Massel (1993), Suh and Park (1995) developed an analytical model that can predict wave reflection from a perforated-wall caisson breakwater mounted on a rubble mound foundation for obliquely incident waves at an arbitrary angle. Suh (1996) showed that Suh and Park's (1995) model, originally developed for a fully perforated wall caisson, can be applied for a partially perforated-wall caisson by assuming that the lower part of the front face of the caisson, which is non-perforated and vertical, is not vertical but has a very steep slope. Kakuno and Nakata (1998) studied the scattering of small amplitude water waves impinging on several rows of vertical cylinders of arbitrary cross section with or without a backwall. In order to verify their method, they compared the theory with laboratory data obtained by other researchers.

Isaacson et al. (1998) suggested the numerical prediction of wave interactions with a thin vertical slotted barriers extending from the water surface to some distance above the seabed. Later, this analysis was extended to double slotted barriers (Isaacson et al., 1999). On the other hand, Isaacson et al. (2000) presented a theoretical analysis and numerical model developed to predict the performance of a perforated-wall caisson breakwater with a rock-filled core. A simplified analytical solution to model the interaction of linear waves with absorbing-type caisson breakwaters, which possess one or two perforated or slotted front faces, was presented by Williams et al. (2000). They concluded that the inclusion of damping effects could improve theoretical predictions significantly.

The previous studies used analytical models that were developed for regular waves, though they include several experimental studies that dealt with irregular waves [e.g., Tanimoto et al. (1976) and Bennett et al. (1992)]. Very recently, Suh et al. (2001) developed an analytical model that predicts the reflection of irregular waves from a perforated-wall caisson. They also conducted laboratory experiments that involved irregular waves of various significant wave heights and periods impinging upon perforated-wall caissons having various wave chamber widths, and compared the experimental results with the analytical model for frequency-averaged reflection coefficients as well as reflected wave spectra.

1.3 Research Objectives and Scope

Though such irregular wave models as the Suh et al.'s (2001) model become available, regular wave models are still in extensive use because of their simplicity. There are several ways to calculate the reflection of irregular waves using a regular wave model. One is to assume the irregular waves as a regular wave whose height and period are the same as the root-mean-squared wave height and significant wave period, respectively, of the irregular waves [e.g., Suh and Park (1995)]. This method inherently assumes that the reflection coefficient is same for all the frequency component of the irregular waves so that the frequency dependent nature of wave reflection cannot be examined. Another way is to use the regular wave model repeatedly for each frequency component of the irregular waves [e.g., Bennett et al. (1992)]. The wave period is determined according to the frequency of each component wave, but it is questionable what wave height should be used. Either the root-mean-squared wave height (or significant wave height) could be used for all the frequencies, or the wave height corresponding to the energy of each frequency component could be used.

In this study, we examine the above-mentioned methods by comparing the calculated results with available experimental data of irregular waves. We use the regular wave model developed by Fugazza and Natale (1992). Even though

this model has been validated using the experimental work of previous authors, we make laboratory experiments in this study to re-validate the model. In the following chapter, the analytical model of Fugazza and Natale (1992) is briefly summarized, and the methods of calculating the reflection of irregular waves using a regular wave model are also included. In chapter 3, the laboratory experiment of regular waves is described, and the regular wave experimental data are compared with the analytical model. In chapter 4, the regular wave model is applied to calculate the irregular wave reflection in the experiments of Suh et al. (2001) and Bennett et al. (1992). The major conclusions and future studies then follow in chapter 5.

CHAPTER 2

THEORETICAL ANALYSIS

2.1 Description of the regular wave model

In this section, the analytical model of Fugazza and Natale (1992) is briefly summarized, which is used in this study. Let us consider the perforated-wall caisson breakwater with vertical slits sketched in Fig. 2.1, in which h is the constant water depth in still water and B is the wave chamber width. The distance between the centers of two adjacent members of the perforated wall is denoted as $2A$ and the width of a slit as $2a$, so that the porosity of the perforated wall is $r = a/A$. The thickness of the perforated wall is denoted as d. The x-axis and y-axis are taken to be normal and parallel, respectively, to the crest line of the perforated wall. The vertical coordinate z is measured vertically upwards from the still water line. Let us assume monochromatic, long-crested and small-amplitude waves normally incident on the breakwater. The wave number of the incident wave is $k = 2\pi/L$, where L denotes the wavelength, and the wave height is H. The linear dispersion relationship is given by $\omega^2 = gk\tanh kh$, where ω is the angular frequency and g is gravitational acceleration.

Neglecting the evanescent waves, the wave potential in the region

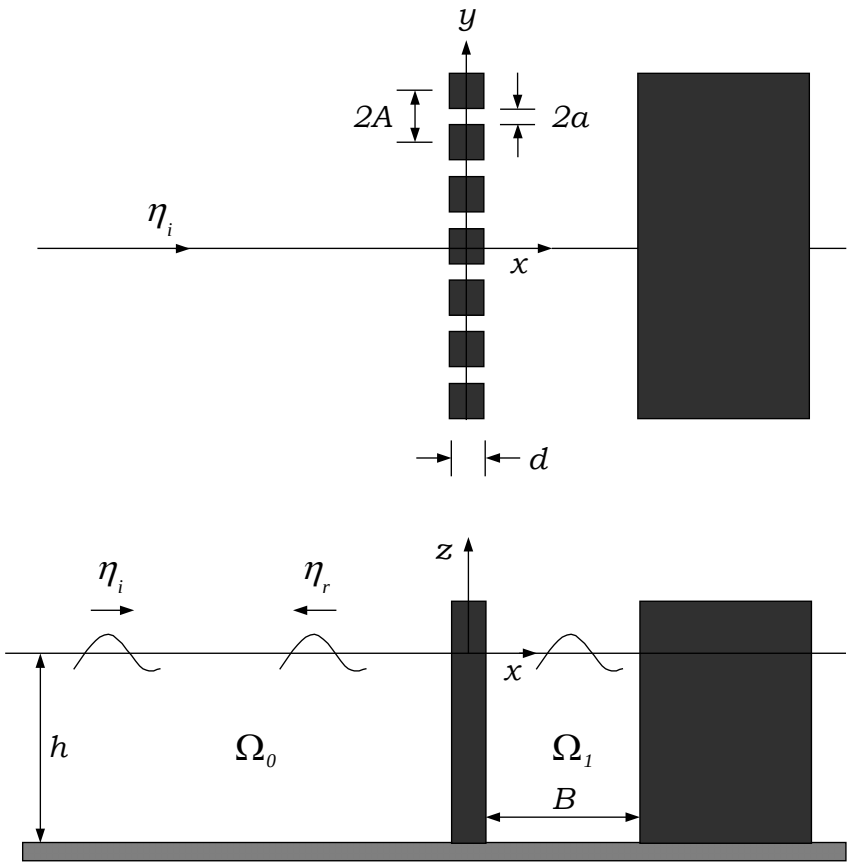

Fig. 2.1 Schematic diagram and coordinate system for calculation of wave reflection from a perforated-wall caisson on a flat bottom

$\Omega_j\,(j=0,1)$ is expressed as

$$\Phi_j = \mathrm{Re}\left\{(a_j + ib_j)\cosh[k(z+h)]e^{i(kx-\omega t)} + (c_j + id_j)\cosh[k(z+h)]e^{i(kx+\omega t)}\right\} \quad (2.1)$$

where $i=\sqrt{-1}$, $a_0 = gH/(2\omega\cosh kh)$, and $b_0 = 0$. At the solid back wall located at $x=B$, the no-flux condition must be satisfied:

$$\frac{\partial\Phi_1}{\partial x} = 0 \quad \text{at} \quad x = B \quad (2.2)$$

At the perforated wall at $x=0$, the following matching conditions must be satisfied:

$$\frac{\partial\Phi_0}{\partial x} - \frac{\partial\Phi_1}{\partial x} = 0 \quad \text{at} \quad x = 0 \quad (2.3)$$

$$\frac{\partial\Phi_1}{\partial t} - \frac{\partial\Phi_0}{\partial t} - \beta\frac{\partial\Phi_0}{\partial x} - \ell\frac{\partial^2\Phi_0}{\partial x\partial t} = 0 \quad \text{at} \quad x = 0 \quad (2.4)$$

where ℓ is the length of the jet flowing through the perforated wall, and β is the linearized dissipation coefficient given by

$$\beta = \frac{8\alpha}{9\pi} H\omega \frac{W}{\sqrt{W^2(R+1)^2 + G^2}} \frac{5 + \cosh 2kh}{2kh + \sinh 2kh} \tag{2.5}$$

where $W = \tan(kB)$, $R = \beta k / \omega$, $P = \ell k$, $G = 1 - PW$ and $\alpha = [1/(rC_c) - 1]^2$ is the energy loss coefficient with C_c being the empirical contraction coefficient at the slit. Mei et al. (1974) suggest using the formula

$$C_c = 0.6 + 0.4r^2 \tag{2.6}$$

for a rectangular geometry like a vertical slit. Note that R in Eq. (2.5) is a function of β. Rearrangement of Eq. (2.5) gives a quartic polynomial of β, which can be solved by the eigenvalue method.

Substituting Eq. (2.1) with $j = 0$ and 1 into Eqs. (2.2) to (2.4) yields a system of linear equations in the unknowns, c_0, d_0, a_1, b_1, c_1, and d_1. Solving these equations, we get

$$c_0 = a_0 \frac{G^2 - W^2(1 - R^2)}{G^2 + W^2(1 + R^2)} \tag{2.7}$$

$$d_0 = -a_0 \frac{2GW}{G^2 + W^2(1 + R^2)} \tag{2.8}$$

Finally the reflection coefficient is obtained as

$$C_r = \frac{\sqrt{c_0^2 + d_0^2}}{a_0} = \frac{[(G^2 + W^2)^2 + W^2R^2(W^2R^2 + 2G^2 - 2W^2)]^{1/2}}{G^2 + W^2(1+R)^2} \tag{2.9}$$

In Eq. (2.4), the jet length, ℓ, represents the inertial resistance at the perforated wall. Fugazza and Natale (1992) assumed that the importance of the local inertia term is feeble, and they took the jet length to be equal to the wall thickness, d. On the other hand, Kakuno and Liu (1993) proposed a blockage coefficient to represent the inertial resistance:

$$C = \frac{d}{2}\left(\frac{A}{a} - 1\right) + \frac{2A}{\pi}\left[1 - \log\left(\frac{4a}{A}\right) + \frac{1}{3}\frac{a}{A} + \frac{281}{180}\left(\frac{a}{A}\right)^4\right] \tag{2.10}$$

Comparison of the models of Fugazza and Natale (1992) and Kakuno and Liu (1993) gives

$$\ell = 2C \tag{2.11}$$

which is much greater than the wall thickness, d, implying that the influence of the inertia resistance term is not so insignificant. For example, for d = 1 cm,

A = 3 cm, and a = 1 cm, the jet length, ℓ, is calculated to be 5.84 cm by the preceding equations, which is almost 6 times the wall thickness. In this study, Eq. (2.11) is used to calculate the jet length, because it gives better agreement with the experimental data than assuming that $\ell = d$.

2.2 Methods of calculation of irregular wave reflection using a regular wave model

There are several ways to calculate the reflection of irregular waves using a regular wave model. In this study, we use two methods. One is to assume the irregular waves as a regular wave whose height and period are the same as the root-mean-squared wave height (or significant wave height) and significant wave period, respectively, of the irregular waves. This method is referred to as Method 1 in this study. This method inherently assumes that the reflection coefficient is same for all the frequency component of the irregular waves so that the frequency dependent nature of wave reflection cannot be examined. The use of either the root-mean-squared wave height or the significant wave height did not give a distinguishable difference, so we used the former in the comparison with the experimental data in chapter 4.

Another way is to use the regular wave model repeatedly for each frequency component of the irregular waves. This method is referred to as Method 2 in

this study. The wave period is determined according to the frequency of each component wave, but it is questionable what wave height should be used. Either the root-mean-squared wave height could be used for all the frequencies, or the wave height corresponding to the energy of each component wave could be used. Both cases will be compared with the experimental data in chapter 4.

In Method 2, the reflection coefficient is calculated differently for each frequency component. The spectral density of the reflected waves for a particular frequency component is calculated by

$$S_r(f) = |C_r(f)|^2 S_i(f) \tag{2.12}$$

where f is the wave frequency and $S_i(f)$ is the incident wave energy spectrum. The frequency-averaged reflection coefficient is then calculated by (Goda, 2000)

$$\overline{C_r} = \sqrt{\frac{m_{0,r}}{m_{0,i}}} \tag{2.13}$$

where $m_{0,i}$ and $m_{0,r}$ are the zeroth moments of the incident and reflected wave spectra, respectively, which are obtained by integrating each spectrum

over the entire frequency range.

CHAPTER 3

LABORATORY EXPERIMENTS AND VALIDATION OF THE REGULAR WAVE MODEL

3.1 Experimental apparatus

Experimental facilities consist of the wave flume, wave gauges and amplifiers, A/D converter, and a personal computer for wave maker control and data acquisition. Characteristics of each equipment are stated below.

3.1.1 Wave Flume and Wave Maker

Experiments were carried out in the wave flume at the Breakwater Laboratory of the Korea Institute of Construction Technology. As shown in Fig. 3.1, the flume is 56-m long, 2-m high, and 1-m wide. Most part of the sidewalls is made of tempered glass so that one can observe the wave motion in the flume. It is equipped with a piston-type wave generator at one end and a wave-absorbing beach at the other. And it is also equipped with a towing carriage for locating wave probes. The wave maker can generate both regular and irregular waves in the frequency range of 0.2 to 2 Hz. The paddle is driven by an AC servo motor and its movement is controlled by a computer system through

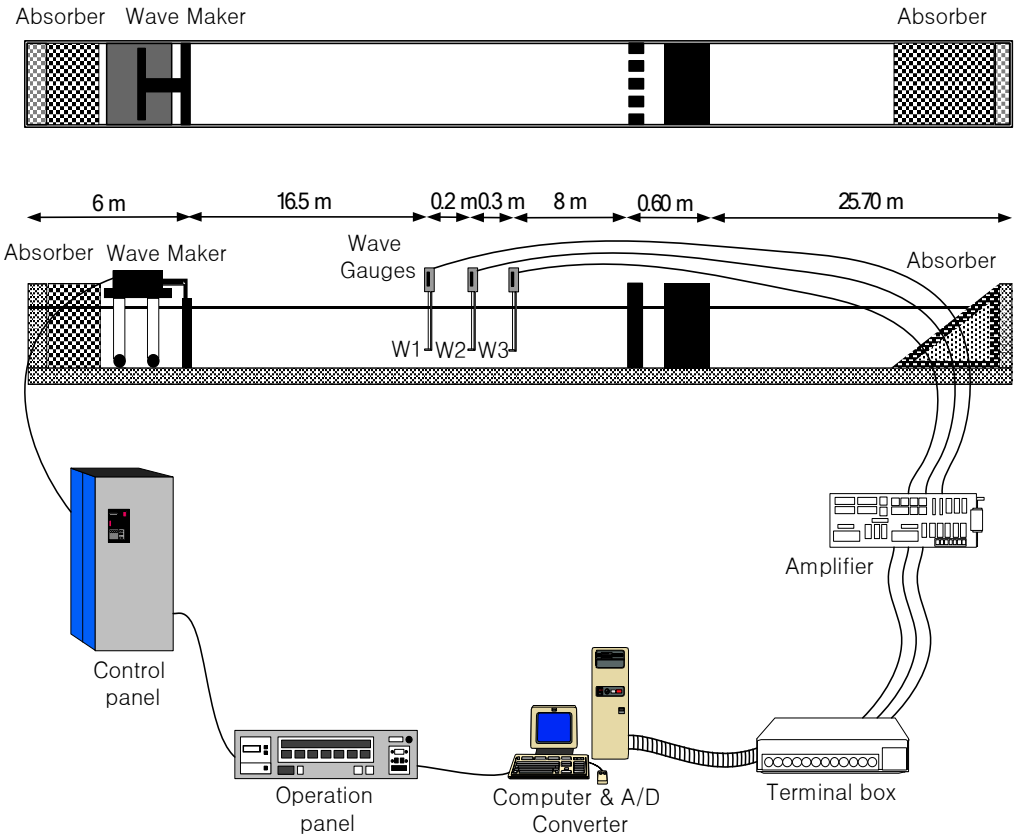

Fig. 3.1. Sketch of experimental setup

electronic voltage signals.

The wave-maker control system contains the so-called reflected wave absorbing filter that can suppress the re-reflection at the wave paddle of the waves reflected from the experimental structure. This is achieved by continuously sensing the reflected waves by a wave gauge attached at the front face of the paddle and correcting the input signal for the movement of the paddle. This makes it possible to carry out an irregular wave test for a long time without accumulation of wave energy in the flume.

Characteristics of the wave maker at the Breakwater Laboratory of the Korea Institute of Construction Technology are detailed in Table 3.1.

3.1.2 Wave Gauges and A/D Converter

Water surface displacements were measured with parallel-wire capacitance-type wave gauges. It comprises of two thin parallel electrodes. When immersed in water, the electrodes measure the conductivity of the instantaneous water volume between them. The conductivity changes proportionately to the variation in water surface elevation.

The signal coming from the gauge exists in the form of analog signal until it gets to an A/D converter. After it passes A/D converter, it is converted to the digital signal. The output voltage can be calibrated in terms of the water surface

Table 3.1 Specification of wave maker

Classification	Specifications
Dimensions of wave paddle	1.0(W) × 2.0(H) m
Maximum depth of water	1.5 m
Maximum wave height	0.9 m(±0.15 m)
Frequency range	0.2~2 Hz
Driving device	AC Servo Motor (5.0 kW)
Control System	A computer system containing the reflected wave absorbing filter
Wave type	Monochromatic waves, Random waves
Instruments	Control panel & Operation panel
Wave generator	Piston type wave generator with active control of reflected wave
Power supply	AC220V, 60Hz, 3Phase(Control) AC110V, 60Hz, 1Phase(Operation Panel)

elevation by varying the depth of immersion of the probe in still water by a measured amount and noting the change in output signal. So, the gauge was calibrated before experiment to ensure the correct conversion of the analog signal to wave height.

The capacitance-type wave gauge used in the present experiment, manufactured by the KENEK Electronics Company, has the 1m-long detector, which can measure the water surface changes within the limit of ± 45 cm. And the amplifier manufactured by the same company was employed to amplify small value signals.

3.1.3 Control System

Wave generator control device is composed of a personal computer, operation panel and the control panel, and each characteristic is as follows. The computer system not only stores the original data but also send control signals to the operation panel in order to make target waves. The operation panel is used to operate the wave generator and controls the reflected wave absorbing filter. The control panel is capable of controlling the main power connected to the wave generator. And it also controls the speed of the servo motor attached to the wave generator with the signals coming from the operation panel.

3.2 Breakwater model and installation

The breakwater model, which is 100 cm wide and 70 cm high, was made from acrylic plates of 1 cm thickness, and the perforated wall consisted of vertical slits with a = 1 cm, A = 3 cm, and d = 1 cm, so that its porosity is 0.333. The breakwater model was placed at a distance of 25 m from the wave maker. In order to measure the incident and reflected waves, three wave gauges were installed as shown in Fig. 3.1. To ensure negligible influence of evanescent waves, gauges were located at more than 8 m away from the breakwater model. To employ the separation technique of incident and reflected waves developed by Park et al. (1992), three gauges were used with spacings of 20 and 30 cm among them.

3.3 Experimental procedure

All the experiments were carried out at a water depth of 40 cm. Four different wave chamber widths were used: 15, 30, 45, and 60 cm. Three different wave heights were used for each wave chamber width, and 4 to 6 different wave periods for each wave height. The target and measured values of the incident wave heights and periods are given in Table 3.2 along with the measured and calculated reflection coefficients.

Table 3.2 Experimental conditions and analyzed data of regular waves

B (cm)	H (cm)	T (s)	H^m (cm)	T^m (s)	C_r^c	C_r^m	Error(%)
15	3	1.0	3.09	0.99	0.701	0.690	1.6
	3	1.2	3.00	1.15	0.848	0.817	3.6
	3	1.4	3.10	1.33	0.913	0.891	2.4
	3	1.6	3.08	1.54	0.952	0.930	2.3
	3	1.8	2.94	1.70	0.965	0.908	6.0
	3	2.0	2.96	1.91	0.977	0.861	11.9
	6	1.2	6.11	1.19	0.764	0.724	5.2
	6	1.4	5.89	1.40	0.875	0.862	1.5
	6	1.6	5.99	1.60	0.923	0.896	3.0
	6	1.8	6.13	1.78	0.946	0.927	2.0
	6	2.0	6.00	1.94	0.959	0.886	7.6
	9	1.4	9.02	1.39	0.821	0.816	0.7
	9	1.6	9.00	1.60	0.888	0.851	4.2
	9	1.8	8.93	1.80	0.926	0.888	5.1
	9	2.0	8.96	2.00	0.948	0.868	8.5
30	3	1.0	2.96	0.99	0.365	0.384	–5.3
	3	1.2	3.00	1.15	0.482	0.550	–14.0
	3	1.4	3.11	1.33	0.613	0.692	–12.8
	3	1.6	3.13	1.54	0.731	0.729	0.2
	3	1.8	3.02	1.70	0.799	0.799	0.1
	3	2.0	3.02	1.91	0.856	0.823	3.8
	6	1.2	6.01	1.19	0.329	0.328	0.2
	6	1.4	5.78	1.40	0.516	0.515	0.2
	6	1.6	6.01	1.60	0.630	0.628	2.4
	6	1.8	6.06	1.78	0.709	0.692	2.4
	6	2.0	6.20	1.94	0.761	0.741	2.6
	9	1.4	11.65	1.39	0.384	0.427	−11.2
	9	1.6	9.15	1.60	0.548	0.560	–2.2
	9	1.8	8.81	1.80	0.649	0.654	−0.7
	9	2.0	8.64	2.00	0.725	0.694	4.3

Table 3.2 (Continued)

B (cm)	H (cm)	T (s)	H^m (cm)	T^m (s)	C_r^c	C_r^m	Error(%)
45	3	1.0	2.92	0.99	0.548	0.549	-0.2
	3	1.2	2.93	1.15	0.420	0.435	−3.6
	3	1.4	3.08	1.33	0.422	0.461	−9.3
	3	1.6	3.13	1.54	0.510	0.552	−8.2
	3	1.8	3.12	1.70	0.584	0.656	−12.3
	3	2.0	3.09	1.91	0.669	0.665	0.6
	6	1.2	6.13	1.19	0.168	0.194	−15.6
	6	1.4	5.90	1.40	0.252	0.291	−15.3
	6	1.6	6.09	1.60	0.362	0.384	−6.2
	6	1.8	6.05	1.78	0.457	0.496	−8.4
	6	2.0	6.27	1.94	0.521	0.547	−5.0
	9	1.4	9.02	1.39	0.143	0.220	−53.8
	9	1.6	9.31	1.60	0.275	0.297	−8.0
	9	1.8	9.10	1.80	0.383	0.399	−4.0
	9	2.0	8.82	2.00	0.477	0.489	−2.6
60	3	1.0	2.88	0.99	0.891	0.873	2.0
	3	1.2	2.88	1.15	0.613	0.595	3.0
	3	1.4	3.04	1.33	0.448	0.457	−1.9
	3	1.6	3.14	1.54	0.411	0.416	−1.2
	3	1.8	2.93	1.70	0.465	0.486	−4.4
	3	2.0	3.05	1.91	0.518	0.531	−2.5
	6	1.2	6.02	1.19	0.377	0.374	0.9
	6	1.4	5.81	1.40	0.215	0.259	−20.3
	6	1.6	6.06	1.60	0.206	0.249	−20.9
	6	1.8	6.05	1.78	0.274	0.292	−6.8
	6	2.0	6.16	1.94	0.336	0.363	−8.1
	9	1.4	8.93	1.39	0.097	0.152	−56.0
	9	1.6	9.11	1.60	0.085	0.167	−95.6
	9	1.8	8.87	1.80	0.192	0.211	−9.7
	9	2.0	8.74	2.00	0.285	0.305	−7.0

The wave measurements were made for 150 s at the sampling rate of 20 Hz immediately after the initiation of wave generation. For the separation of incident and reflected waves, we have to use the wave records that include the incident waves and the reflected waves from the breakwater but do not include the re-reflected waves from the wave paddle. The leading wave propagates at the speed of group velocity. Therefore, the time for the leading wave generated by the wave maker to be reflected from the breakwater and arrive at the location of the wave gauges can be calculated approximately. By examining the plotted wave records and using the approximate arrival time of the first reflected wave, we selected a fraction of the wave records of length of 10 wave periods that includes only the incident waves and the reflected waves from the breakwater. It was then used for the separation of incident and reflected waves. An example is illustrated in Fig. 3.2.

3.4 Validation of the regular wave model

In this section, the regular wave model is validated by comparing the computational results with the experimental measurements. The measured and calculated reflection coefficients are given in Table 3.2 along with the relative error, which was calculated by

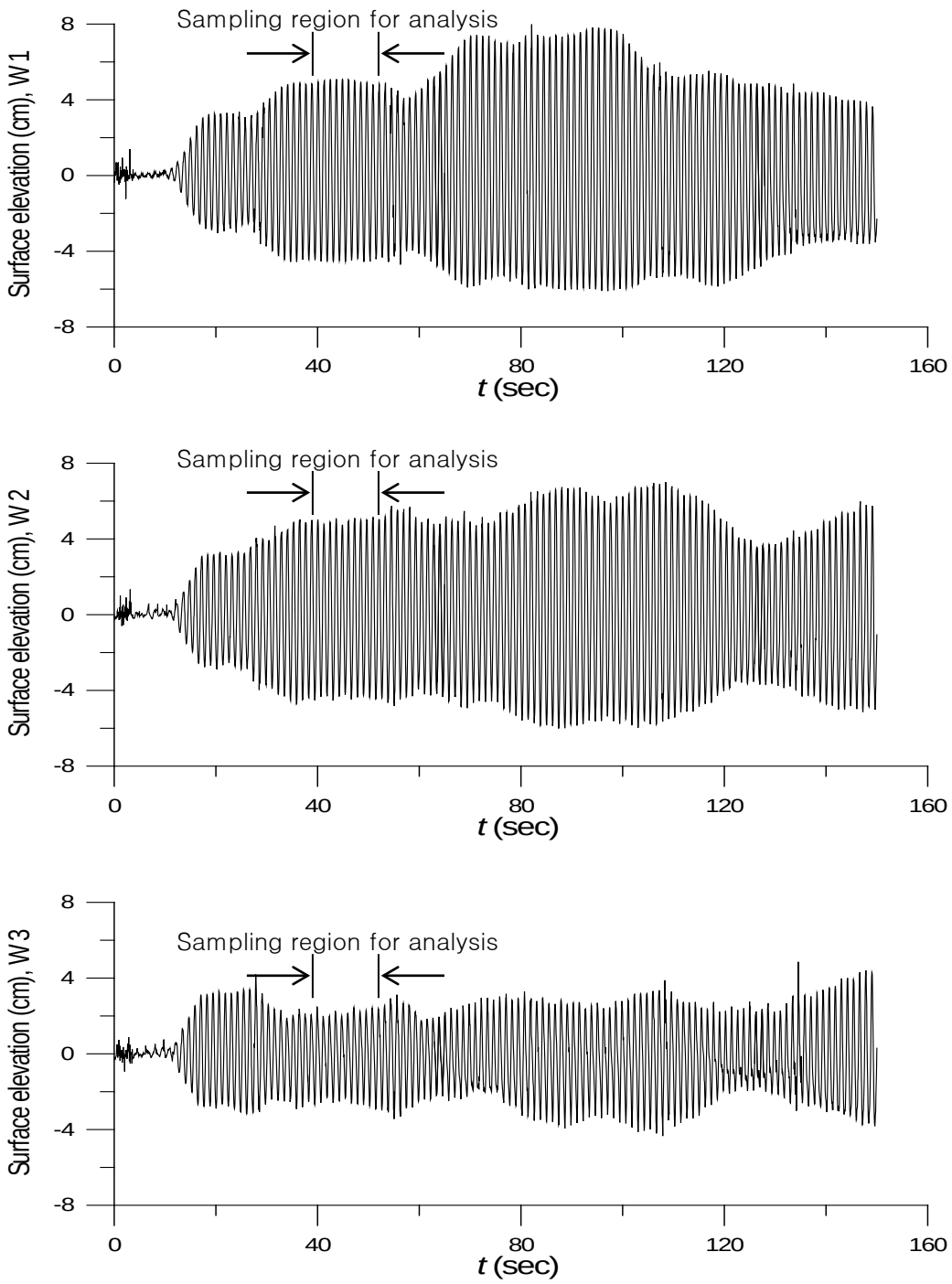

Fig. 3.2. An example of wave records in case of B=15 cm, H=3 cm, T=1.2 sec

$$\text{Error} = \frac{C_r^c - C_r^m}{C_r^c} \times 100\% \tag{3.1}$$

where the superscripts c and m denote calculation and measurement, respectively. The examination of the results given in Table 3.2 suggests that for steeper waves, the model predicts smaller reflection coefficients in both measurement and calculation. This seems to be attributed to the increase of energy loss with the increased wave steepness. The contraction coefficient, C_c, is calculated to be 0.644 by Eq. (2.6), but slight improvement was obtained using $C_c = 0.7$ instead of $C_c = 0.644$ as will be shown in Fig. 3.3. Therefore, $C_c = 0.7$ is used in the computational results presented hereinafter.

Comparison of the measured and calculated reflection coefficients is shown in Fig. 3.3. The results of $C_c = 0.7$ show slightly better agreement than those of $C_c = 0.644$. Here we use the index of agreement proposed by Willmott (1981) as a measure of the degree to which a model's predictions are error-free:

$$I_a = 1 - \frac{\sum_{i=1}^{N} (P_i - O_i)^2}{\sum_{i=1}^{N} (\left|P_i - \overline{O}\right| + \left|O_i - \overline{O}\right|)^2} \tag{3.2}$$

where $\overline{O}$ is the mean of the observed variates O_i, and P_i, $i = 1$ to N, are the predicted variates. The values for I_a vary between 0 and 1.0, where 1.0

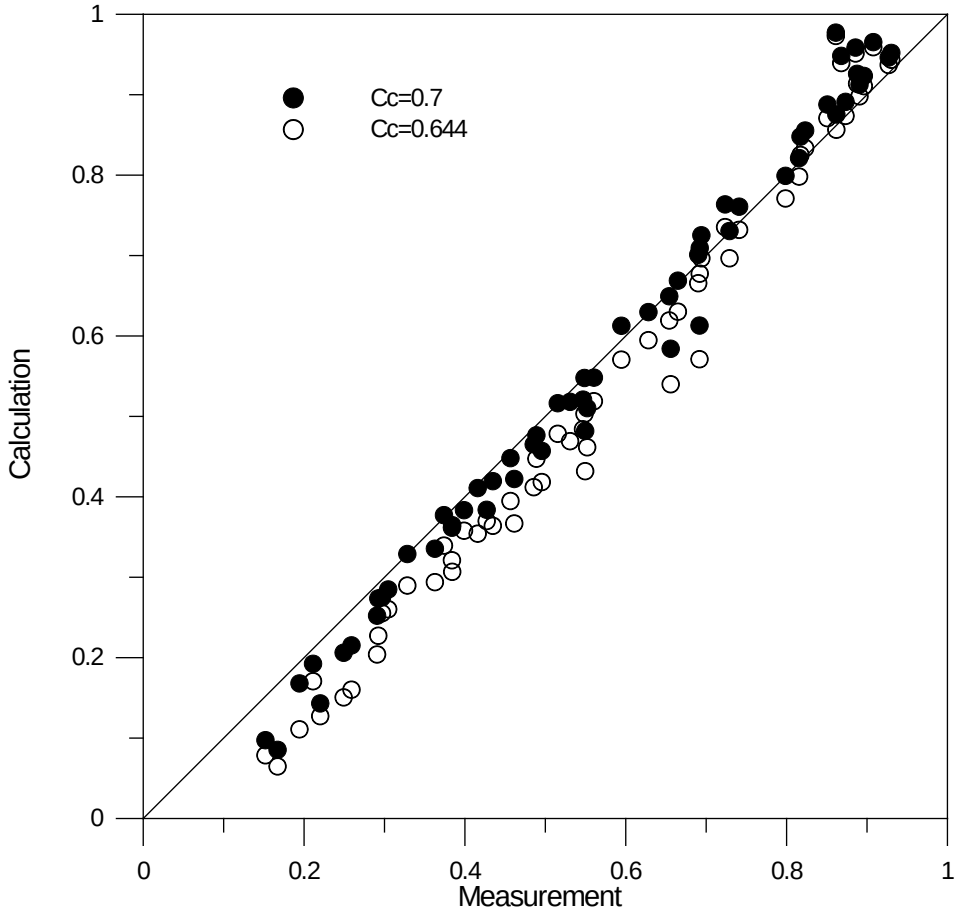

Fig. 3.3. Comparison of reflection coefficients of regular waves between measurement and calculation

indicates perfect agreement between observation and prediction, and 0 connotes complete disagreement. The indices of agreement in cases of $C_c = 0.7$ and $C_c = 0.644$ are 0.994 and 0.985, respectively.

Though the overall agreement is acceptable when we use $C_c = 0.7$, the model somewhat over-predicts the reflection coefficients at larger values, while under-predicting them at smaller values. These differences may be attributed to the neglect of the evanescent waves near the breakwater [see Park et al. (2000) and Suh et al. (2001)].

To see in detail the effect of the evanescent waves, we calculated the energy loss coefficients, C_l, which is related to the reflection coefficient by

$$C_l = 1 - C_r^{\,2} \tag{3.3}$$

In Fig. 3.4 are shown the values of C_l^c / C_l^m as a function of C_r^m, in which again the superscripts c and m denote calculation and measurement, respectively. As the reflection coefficient increases, the calculated energy loss becomes less than the measured one. This discrepancy may be due to the assumption of 'wide spacing approximation' which neglects the evanescent waves near the slit wall.

The evanescent waves may increase the energy loss through the gap

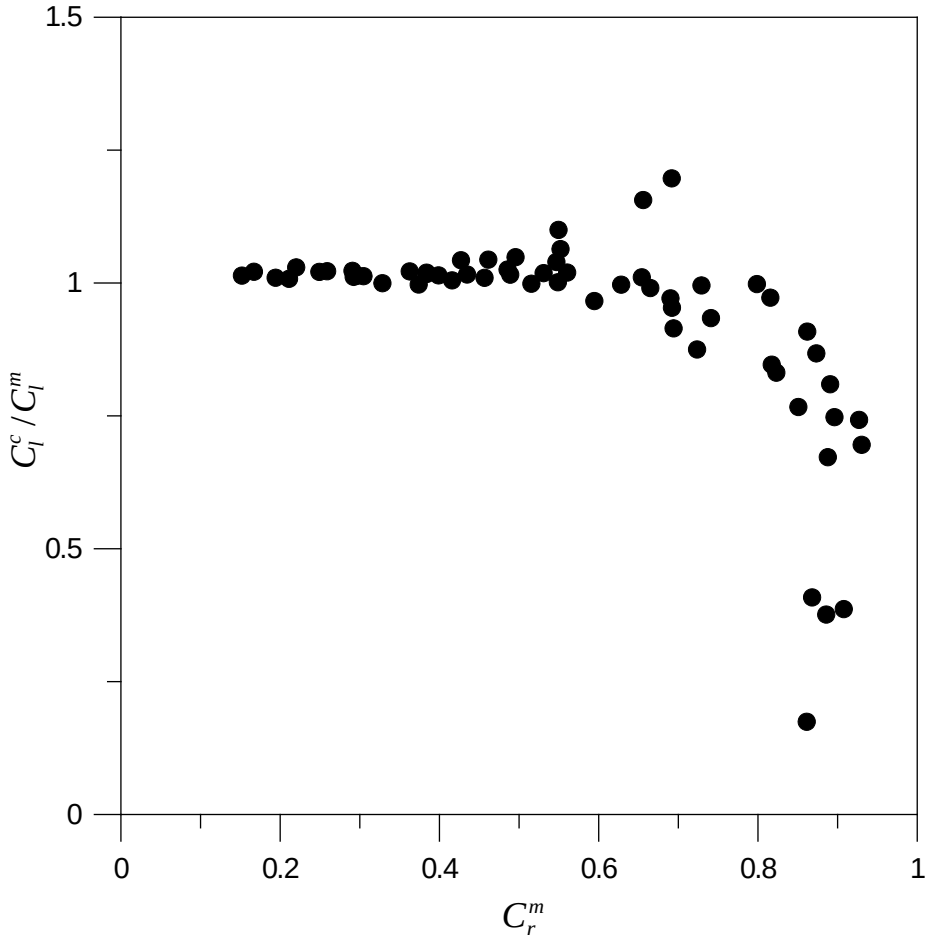

Fig. 3.4. Values of C_l^c / C_l^m as a function of C_r^m

between the cylinders, and their effect may increase with increasing reflection. Therefore, the present model which neglects the evanescent waves near the breakwater, may under-predict the energy loss coefficients, and hence over-predict the reflection coefficients, inversely.

On the other hand, it is well known that the wave reflection from a perforated-wall caisson breakwater is related to the relative ratio of the chamber width to the wavelength. For a perforated-wall caisson lying on a flat bottom, Fugazza and Natale (1992) showed that the reflection of waves normally incident to the caisson is minimized when the wave chamber width is about one quarter of the wavelength, i.e., B/L = 0.25. The reason is that when B/L = 0.25 the reflection of the perforated wall and the reflection of the impermeable wall are in opposite phase. So, the resonant condition for the perforated-wall caisson breakwater is given by

$$B = \frac{2n+1}{4} L \tag{3.4}$$

where n is an integer.

But, in practice, the reflection coefficients are minimized when B/L is less than 0.25 as shown in Fig. 3.5 to 3.7. This is due to the effect the inertial resistance [see Suh. (1996)]. As shown in chaper 2, we consider the influence of inertia term by setting $\ell = 2C$ in Eq. (2.11).

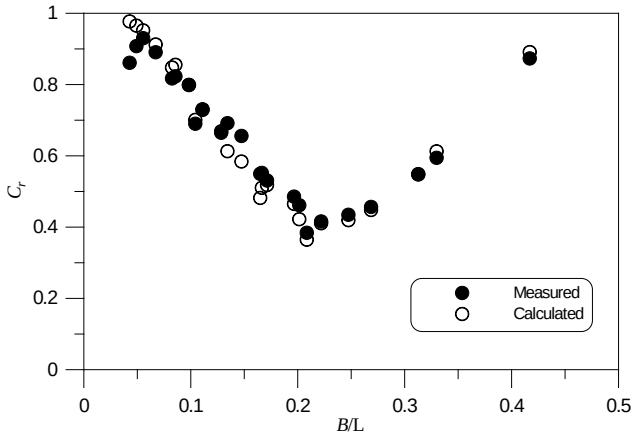

Fig. 3.5. Variation of reflection coefficients with respect to *B*/L (*H* = 3 cm)

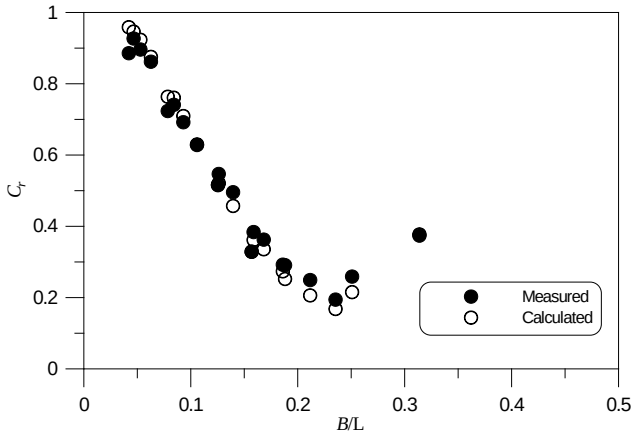

Fig. 3.6. Variation of reflection coefficients with respect to *B*/L (*H* = 6 cm)

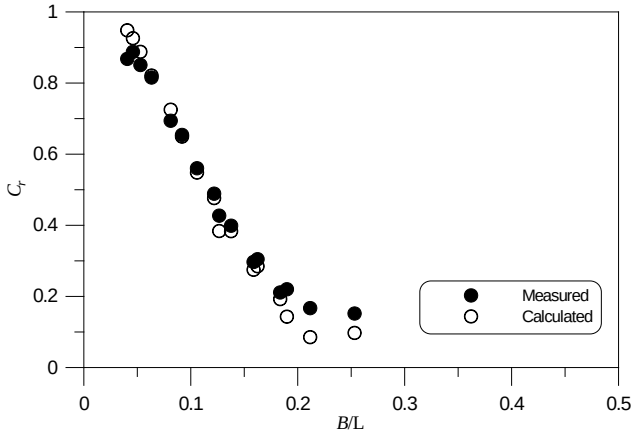

Fig. 3.7. Variation of reflection coefficients with respect to *B*/L (*H* = 9 cm)

CHAPTER 4

APPLICATION OF THE REGULAR WAVE MODEL TO CALCULATION OF IRREGULAR WAVE REFLECTION

4.1 Comparison with the experiment of Suh et al. (2001)

Suh et al. (2001) carried out laboratory experiments for irregular wave reflection from perforated-wall caisson breakwaters using the same breakwater models and wave flume as those used in the present study. The incident wave spectrum used in the experiment was the Bretschneider-Mitsuyasu spectrum given by

$$S_i(f) = 0.205 H_s^2 T_s (T_s f)^{-5} \exp[-0.75(T_s f)^{-4}] \tag{4.1}$$

where H_s and T_s are the significant wave height and period, respectively. They used the target significant wave heights and periods that are the same as the target values of the regular waves in Table 3.2. The experimental results of Suh et al. are listed in Table 4.1. The calculated values, $\overline{C}_r^c$, in Table 4.1 were obtained by Suh et al.'s (2001) irregular wave model. Table 4.1 also contains the measured values of significant wave heights and periods, H_s^m and T_s^m.

Table 4.1 Experimental conditions and analyzed data of Suh et al. (2001)

B (cm)	H_s (cm)	T_s (s)	H_s^m (cm)	T_s^m (s)	$\overline{C}_r^c$	$\overline{C}_r^m$	Error(%)
15	3	1.0	3.54	0.98	0.711	0.760	–7.0
	3	1.2	3.16	1.26	0.832	0.800	3.8
	3	1.4	2.90	1.36	0.866	0.834	3.7
	3	1.6	2.94	1.65	0.931	0.884	5.1
	3	1.8	2.85	1.76	0.946	0.868	8.3
	3	2.0	3.04	2.00	0.966	0.885	8.4
	6	1.2	6.41	1.23	0.737	0.742	–0.7
	6	1.4	5.95	1.35	0.800	0.782	2.3
	6	1.6	5.95	1.64	0.884	0.855	3.4
	6	1.8	5.90	1.78	0.910	0.850	6.6
	6	2.0	6.01	2.02	0.941	0.864	8.2
	9	1.4	8.94	1.39	0.768	0.772	–0.5
	9	1.6	9.25	1.63	0.842	0.831	1.3
	9	1.8	8.92	1.77	0.878	0.830	5.5
	9	2.0	8.89	2.00	0.915	0.871	4.8
30	3	1.0	3.13	0.92	0.631	0.671	–6.3
	3	1.2	3.06	1.21	0.638	0.635	0.6
	3	1.4	3.13	1.43	0.691	0.694	–0.4
	3	1.6	2.94	1.63	0.767	0.749	2.4
	3	1.8	2.93	1.78	0.806	0.760	5.6
	3	2.0	2.95	2.00	0.851	0.805	5.4
	6	1.2	6.29	1.24	0.500	0.553	−10.6
	6	1.4	6.11	1.41	0.568	0.605	–6.6
	6	1.6	5.95	1.63	0.652	0.679	−4.2
	6	1.8	5.89	1.77	0.698	0.682	2.2
	6	2.0	5.92	2.00	0.762	0.728	4.6
	9	1.4	9.43	1.39	0.501	0.560	−11.8
	9	1.6	9.02	1.62	0.583	0.623	–6.9
	9	1.8	9.10	1.78	0.629	0.639	−1.5
	9	2.0	8.99	1.98	0.700	0.682	2.5

Table 4.1 (Continued)

B (cm)	H_s (cm)	T_s (s)	H_s^m (cm)	T_s^m (s)	$\overline{C}_r^c$	$\overline{C}_r^m$	Error(%)
45	3	1.0	3.25	0.87	0.608	0.703	–15.6
	3	1.2	3.10	1.23	0.577	0.593	−2.8
	3	1.4	3.10	1.44	0.605	0.618	−2.1
	3	1.6	2.84	1.61	0.634	0.655	−3.2
	3	1.8	2.94	1.75	0.666	0.661	0.8
	3	2.0	2.97	2.00	0.717	0.693	3.3
	6	1.2	6.07	1.21	0.425	0.475	−11.9
	6	1.4	6.08	1.41	0.466	0.518	−11.2
	6	1.6	5.77	1.58	0.483	0.544	−12.5
	6	1.8	6.00	1.72	0.512	0.548	−6.9
	6	2.0	5.93	1.98	0.583	0.593	−1.8
	9	1.4	9.35	1.40	0.385	0.469	−21.8
	9	1.6	8.63	1.58	0.410	0.487	−18.6
	9	1.8	9.15	1.76	0.445	0.497	−11.8
	9	2.0	9.19	1.95	0.509	0.540	−6.1
60	3	1.0	3.22	1.04	0.692	0.703	–1.6
	3	1.2	3.07	1.23	0.639	0.623	2.5
	3	1.4	2.97	1.40	0.605	0.620	−2.5
	3	1.6	2.93	1.64	0.601	0.610	−1.5
	3	1.8	2.93	1.81	0.602	0.609	−1.2
	3	2.0	2.97	2.01	0.627	0.621	1.1
	6	1.2	6.24	1.22	0.507	0.514	−1.5
	6	1.4	6.00	1.40	0.452	0.511	−13.2
	6	1.6	5.91	1.64	0.434	0.490	−12.7
	6	1.8	5.92	1.77	0.436	0.489	−12.1
	6	2.0	5.96	2.00	0.469	0.513	−9.5
	9	1.4	9.18	1.40	0.399	0.461	−15.6
	9	1.6	8.87	1.58	0.370	0.452	−22.4
	9	1.8	8.84	1.75	0.353	0.420	−19.0
	9	2.0	9.09	1.95	0.383	0.454	−18.6

These were calculated by zero-crossing analysis of the time series of surface elevation of the incident waves obtained by the method of Park et al. (1992). In the following calculation, the measured values of significant wave heights and periods (or the measured incident and reflected wave spectra) are used.

The reflection coefficients calculated by Method 1, denoted as $\overline{C}_r^1$, are listed in Table 4.2. Fig. 4.1 shows the comparison between measurement and calculation. The model considerably over-predicts the reflection coefficients at larger values, while largely under-predicting them at smaller values. The index of agreement which is defined in chapter 3 is equal to 0.903.

The frequency-averaged reflection coefficients, $\overline{C}_r^2$, calculated by Method 2 using the root-mean-squared wave height for all the frequencies are presented in Table 4.2. Fig. 4.2 shows the comparison of the reflection coefficients between measurement and calculation. The model somewhat over-predicts the reflection coefficients at larger values, but the overall agreement is acceptable. In this case, the index of agreement is calculated to be 0.978. To examine the frequency dependency nature of wave reflection in detail, the measured and calculated spectra of incident and reflected waves were plotted. All the cases are presented in the Appendix A. Here, two of them, which give the best and worst agreement between measurement and calculation for the frequency-averaged reflection coefficients, are presented in Fig 4.3 and 4.4. Fig 4.3 shows the results for the case of $H_s \approx 6\,\text{cm}$, $T_s \approx 1.8\,\text{s}$ and $B = 60\,\text{cm}$, for which the

Table 4.2 Calculated reflection coefficients using regular wave model with the data of Suh et al. (2001).

B (cm)	H_s^m (cm)	T_s^m (s)	$\overline{C}_r^m$	$\overline{C}_r^1$	Error(%)	$\overline{C}_r^2$	Error(%)	$\overline{C}_r^3$	Error(%)
15	3.54	0.98	0.760	0.724	-5.0	0.736	-3.2	0.968	21.5
	3.16	1.26	0.800	0.918	12.8	0.851	6.0	0.986	18.8
	2.90	1.36	0.834	0.945	11.7	0.883	5.6	0.989	15.7
	2.94	1.65	0.884	0.974	9.3	0.938	5.8	0.995	11.2
	2.85	1.76	0.868	0.980	11.4	0.953	8.9	0.996	12.9
	3.04	2.00	0.885	0.987	10.3	0.969	8.7	0.998	11.3
	6.41	1.23	0.742	0.834	11.0	0.771	3.8	0.969	23.4
	5.95	1.35	0.782	0.891	12.2	0.826	5.3	0.979	20.1
	5.95	1.64	0.855	0.948	9.8	0.899	5.0	0.990	13.7
	5.90	1.78	0.850	0.961	11.6	0.924	8.0	0.993	14.4
	6.01	2.02	0.864	0.975	11.4	0.947	8.8	0.996	13.2
	8.94	1.39	0.772	0.863	10.5	0.780	3.4	0.972	20.5
	9.25	1.63	0.831	0.920	9.6	0.866	4.0	0.985	15.6
	8.92	1.77	0.830	0.942	11.9	0.896	7.4	0.989	16.1
	8.89	2.00	0.871	0.962	9.5	0.926	6.0	0.993	12.3
30	3.13	0.92	0.671	0.447	-50.1	0.682	1.7	0.960	30.1
	3.06	1.21	0.635	0.617	-2.8	0.687	7.6	0.961	34.0
	3.13	1.43	0.694	0.744	6.8	0.736	5.7	0.968	28.3
	2.94	1.63	0.749	0.832	10.0	0.799	6.3	0.977	23.4
	2.93	1.78	0.760	0.871	12.7	0.833	8.7	0.982	22.5
	2.95	2.00	0.805	0.908	11.4	0.869	7.4	0.986	18.4
	6.29	1.24	0.553	0.452	-22.3	0.550	-0.5	0.927	40.4
	6.11	1.41	0.605	0.590	-2.6	0.616	1.7	0.942	35.7
	5.95	1.63	0.679	0.715	4.9	0.695	2.2	0.957	29.0
	5.89	1.77	0.682	0.771	11.5	0.735	7.2	0.964	29.2
	5.92	2.00	0.728	0.835	12.8	0.792	8.1	0.973	25.2
	9.43	1.39	0.560	0.478	-17.2	0.542	-3.2	0.916	38.9
	9.02	1.62	0.623	0.628	0.8	0.626	0.5	0.937	33.5
	9.10	1.78	0.639	0.699	8.6	0.669	4.6	0.946	32.5
	8.99	1.98	0.682	0.769	11.3	0.734	7.1	0.960	29.0

* Note : $\overline{C}_r^1$ denotes the calculated reflection coefficient by Method 1. $\overline{C}_r^2$ denotes the calculated reflection coefficient by Method 2 using the root-mean squared wave height for all the frequencies. $\overline{C}_r^3$ denotes the calculated reflection coefficient by Method 2 using the wave height corresponding to the energy of each frequency component .

Table 4.2 (Continued)

B (cm)	H_s^m (cm)	T_s^m (s)	$\overline{C}_r^m$	$\overline{C}_r^1$	Error(%)	$\overline{C}_r^2$	Error(%)	$\overline{C}_r^3$	Error(%)
45	3.25	0.87	0.703	0.828	15.1	0.644	-9.2	0.949	25.9
	3.10	1.23	0.593	0.504	-17.5	0.634	6.5	0.950	37.6
	3.10	1.44	0.618	0.565	-9.4	0.657	6.0	0.954	35.2
	2.84	1.61	0.655	0.655	0.0	0.686	4.5	0.958	31.6
	2.94	1.75	0.661	0.698	5.3	0.714	7.3	0.962	31.3
	2.97	2.00	0.693	0.772	10.2	0.755	8.1	0.967	28.3
	6.07	1.21	0.475	0.287	-65.6	0.481	1.2	0.908	47.7
	6.08	1.41	0.518	0.353	-46.8	0.518	0.0	0.918	43.6
	5.77	1.58	0.544	0.457	-19.0	0.537	-1.3	0.922	41.1
	6.00	1.72	0.548	0.516	-6.2	0.567	3.5	0.928	41.0
	5.93	1.98	0.593	0.627	5.5	0.629	5.7	0.939	36.9
	9.35	1.40	0.469	0.220	-112.9	0.426	-10.1	0.880	46.7
	8.63	1.58	0.487	0.350	-39.1	0.458	-6.2	0.891	45.4
	9.15	1.76	0.497	0.432	-15.0	0.493	-0.9	0.896	44.5
	9.19	1.95	0.540	0.517	-4.4	0.552	2.1	0.913	40.8
60	3.22	1.04	0.703	0.826	14.9	0.718	2.1	0.965	27.2
	3.07	1.23	0.623	0.603	-3.5	0.683	8.7	0.958	34.9
	2.97	1.40	0.620	0.537	-15.4	0.653	5.0	0.951	34.8
	2.93	1.64	0.610	0.553	-10.2	0.650	6.3	0.947	35.6
	2.93	1.81	0.609	0.594	-2.6	0.653	6.7	0.948	35.7
	2.97	2.01	0.621	0.645	3.8	0.673	7.7	0.950	34.7
	6.24	1.22	0.514	0.421	-22.3	0.554	7.2	0.920	44.1
	6.00	1.40	0.511	0.319	-60.5	0.503	-1.6	0.910	43.8
	5.91	1.64	0.490	0.338	-45.0	0.487	-0.5	0.902	45.7
	5.92	1.77	0.489	0.378	-29.4	0.489	0.0	0.902	45.8
	5.96	2.00	0.513	0.460	-11.5	0.517	0.8	0.907	43.4
	9.18	1.40	0.461	0.180	-156.2	0.441	-4.5	0.874	47.3
	8.87	1.58	0.452	0.189	-139.6	0.413	-9.7	0.865	47.7
	8.84	1.75	0.420	0.252	-66.8	0.399	-5.4	0.860	51.2
	9.09	1.95	0.454	0.329	-38.0	0.425	-6.9	0.867	47.6

* Note : $\overline{C}_r^1$ denotes the calculated reflection coefficient by Method 1. $\overline{C}_r^2$ denotes the calculated reflection coefficient by Method 2 using the root-mean squared wave height for all the frequencies. $\overline{C}_r^3$ denotes the calculated reflection coefficient by Method 2 using the wave height corresponding to the energy of each frequency component .

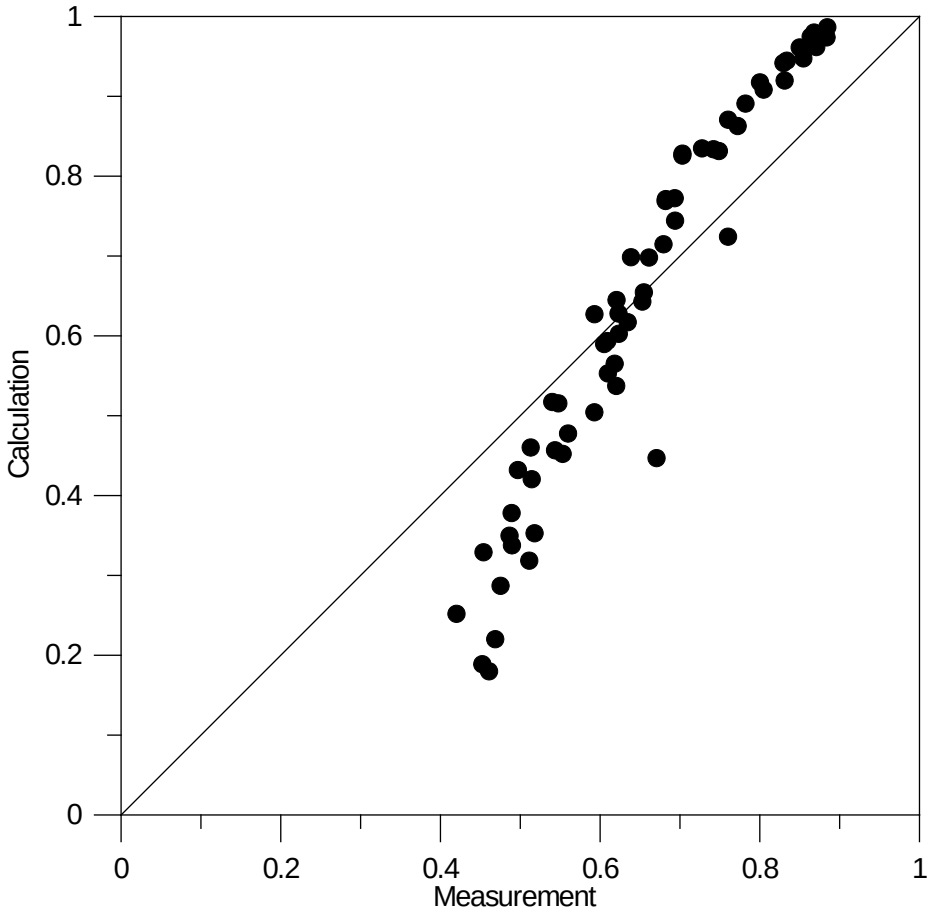

Fig. 4.1. Comparison of reflection coefficients between measurement and calculation (Method 1) for experimental data of Suh et al. (2001)

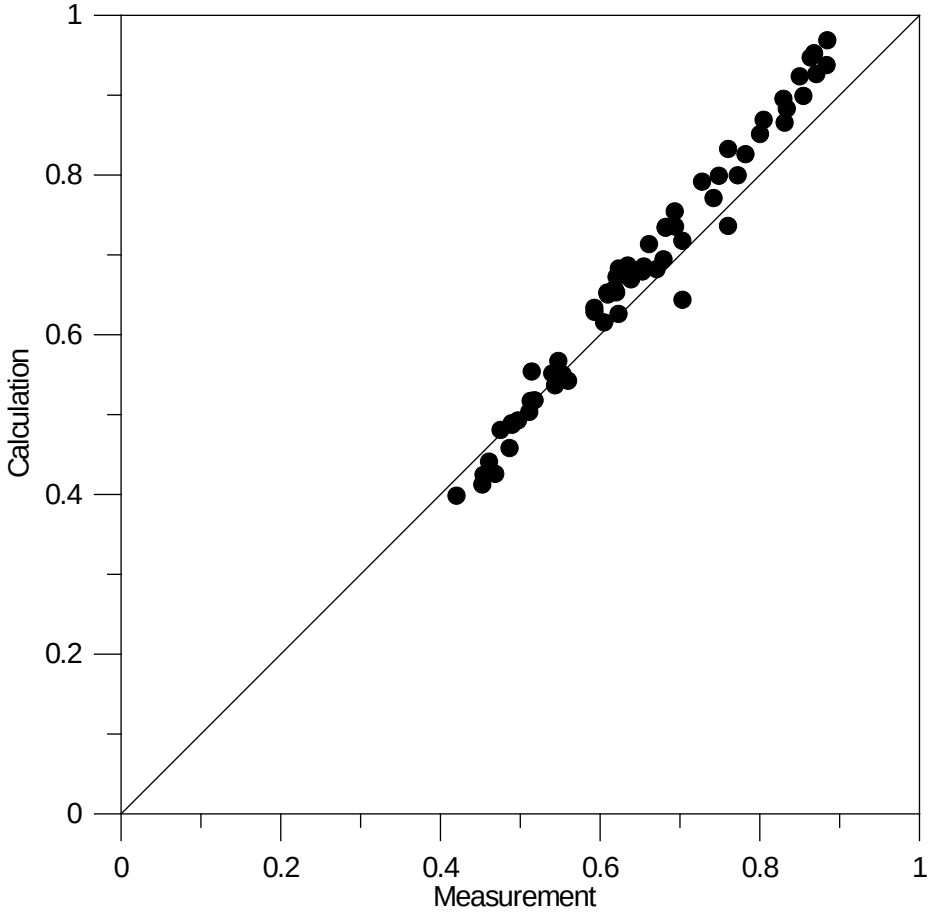

Fig. 4.2. Same as Fig. 4.1, but for Method 2 using the root-mean-squared wave height for all the frequencies.

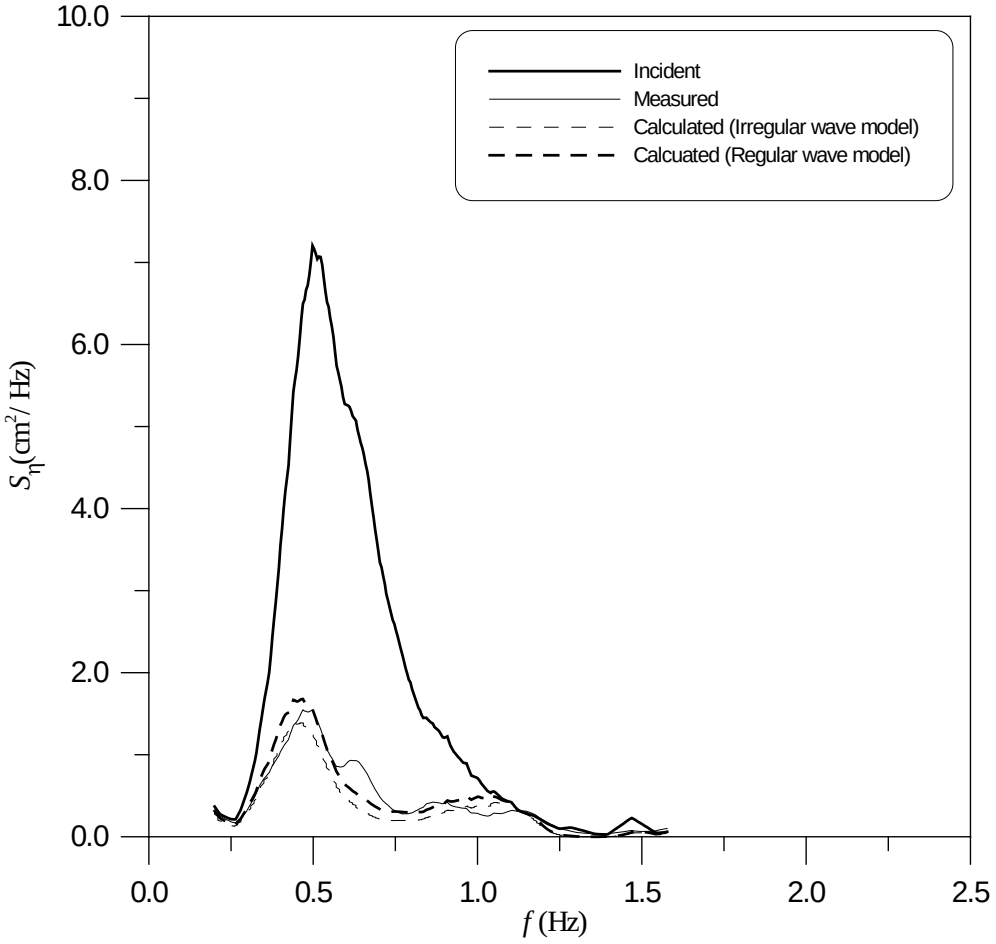

Fig. 4.3. Measured and calculated spectra of incident and reflected waves for the case of $H_s \approx 6$ cm, $T_s \approx 1.8$ s and $B = 60$ cm: thick solid line = incident wave, thin solid line = measured reflected wave, thick dashed line = calculated reflected wave by regular wave model, thin dashed line = calculated reflected wave by irregular wave model of Suh et al. (2001)

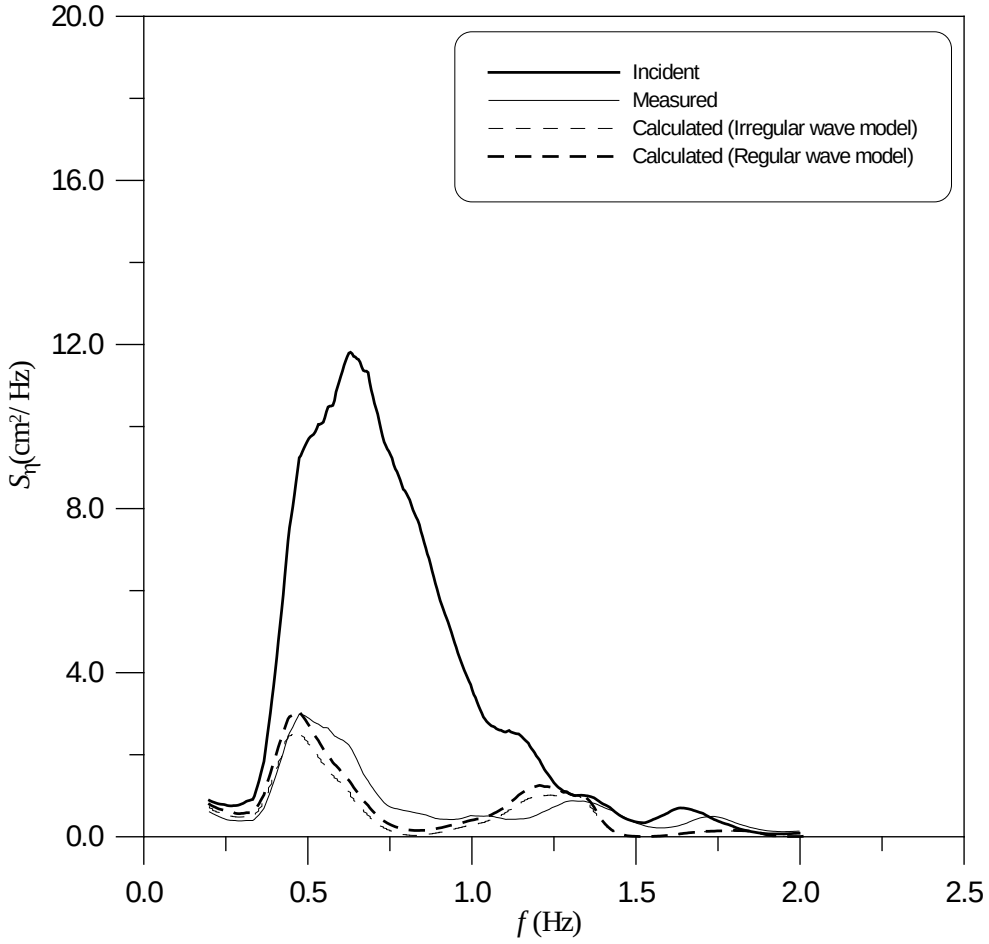

Fig. 4.4. Same as Fig. 4.3, but for $H_s \approx 9\,\text{cm}$, $T_s \approx 1.4\,\text{s}$ and $B = 45\,\text{cm}$.

error is 0.02%. Agreement between measurement and calculation is quite good. On the other hand, Fig 4.4 shows the results for the case of $H_s \approx 9\,\text{cm}$, $T_s \approx 1.4\,\text{s}$ and $B = 45\,\text{cm}$, for which the error is -10.1%. The details show some difference depending on the frequency, but the overall agreement is still acceptable.

There is a little difference between regular wave model and irregular wave model. Without exception in all the cases, the regular wave model gives a little larger frequency-averaged reflection coefficient than the irregular wave model. This can be confirmed by comparing the value of $\overline{C}_r^c$ in Table 4.1 with the value of $\overline{C}_r^2$ in Table 4.2. Also, note that the cases of best and worst agreement of the regular wave model do not coincide with those of the irregular wave model. And in Figs 4.3 and 4.4 (and some figures in the Appendix A) is also shown a frequency dependent oscillatory behavior. As referred in chapter 3, the wave reflection from a perforated-wall caisson breakwater depends primarily upon the wave chamber width relative to the wavelength. As a result, for irregular waves, the reflected wave spectrum oscillates with the frequency that is related to the wavelength [see Suh et al. (2001)].

Fig. 4.5 shows the results of Method 2 using the wave height corresponding to the energy of each frequency component, which is much smaller than the root-mean-squared wave height. The model severely over-predicts the reflection coefficients because the energy dissipation at the perforated wall, which is

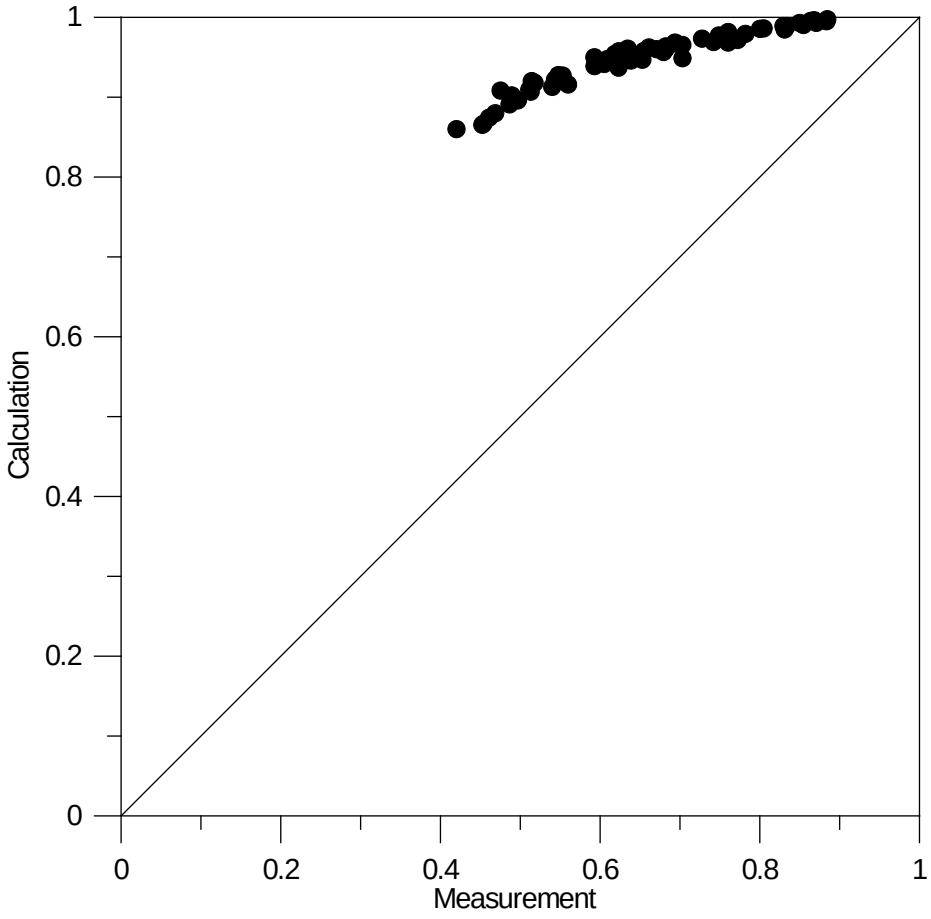

Fig. 4.5. Same as Fig. 4.1, but for Method 2 using the wave height corresponding to each frequency component.

proportional to the wave height, is calculated to be very small so that most wave energy is reflected from the breakwater. The index of agreement in this case is only 0.437. The frequency-averaged reflection coefficients, $\overline{C}_r^3$, calculated by this method are presented in Table 4.2.

4.2 Comparison with the experiment of Bennett et al. (1992)

The laboratory experiment of Suh et al. (2001) is of relative small scale. At a larger scale of 1:15, Bennett et al. (1992) made a laboratory experiment for irregular wave reflection from a slotted wavescreen breakwater both with and without a solid backing wall. Here we utilize the experimental data in the cases with a backing wall. The experimental conditions are given below referring to the prototype. All the tests were carried out at a water depth of 8.6 m for two spectra corresponding to wave conditions which were likely to occur at the possible location. Spectrum A covered frequencies equivalent to wave periods of 4.5 to 14 s and spectrum B covered 2.9 to 6.2 s (see Fig. 4.6). Significant wave heights corresponding to spectrum A and B are 0.91 and 1.41 m, respectively. Three different wave chamber widths were used: 5, 10 and 15 m. And three different porosities of the slit wall were used for each spectrum. However, some values needed for calculation are not presented in Bennett et al. (1992)'s paper. Therefore we assume those values as reasonable ones which are

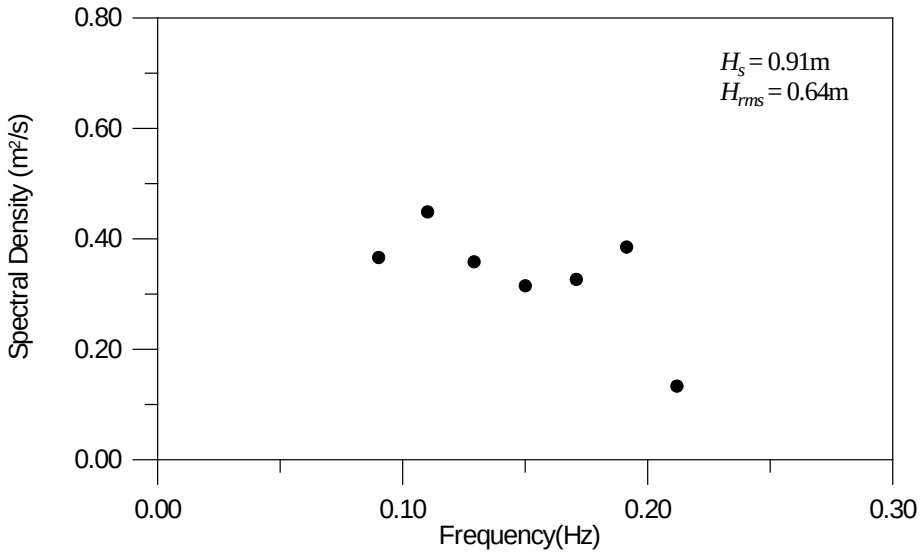

(a)

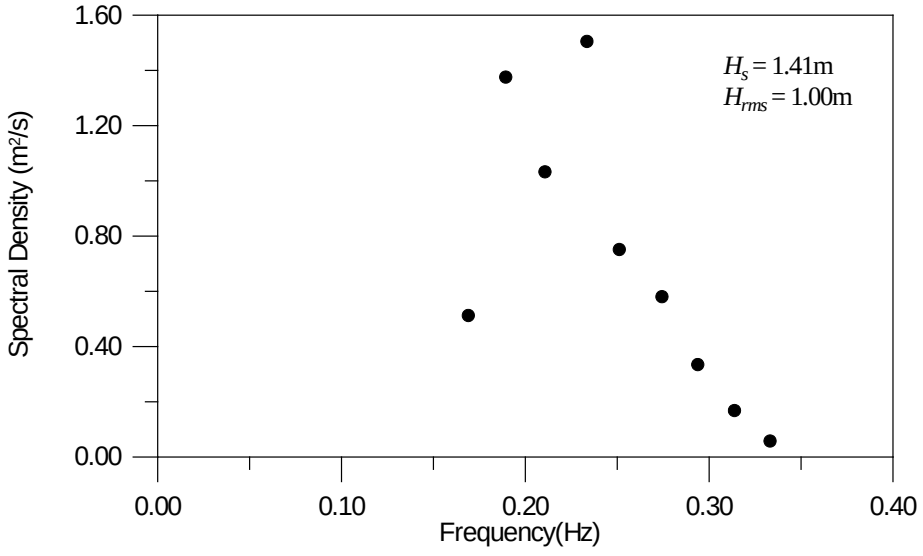

(b)

Fig. 4.6. Spectral energy density vs. frequency: (a) Spectrum A; (b) Spectrum B

often used in practical case. The half distance between the centers of two adjacent members of slit walls, A, and the thickness of the perforated-wall, d, are assumed to be 0.6 m and 15 cm, respectively. And the half width of a slit, a, is determined according to porosity.

To compare the theoretical values with the measured values, the calculation by Method 2 using the root-mean-squared wave height for all the frequencies was made. In the previous section, this method has been proved to be the most error-free. Figs. 4.7 to 4.11 show the comparison between measurement and calculation for various porosities and various wave chamber widths. Though the model somewhat over-predicts the reflection coefficients in some cases, good agreement is found in all the cases. Figs. 4.7, 4.8 and 4.9 show comparisons for a fixed porosity and various wave chamber widths. Each curve in the figures shows the aforementioned frequency dependent oscillatory behavior. It has the peaks at frequencies given by

$$f = \sqrt{\frac{ng}{4\pi B}\tanh\left(\frac{n\pi h}{B}\right)} \tag{4.2}$$

where n is an integer and B is the wave chamber width [see Bennett et al. (1992)]. The preceding equation is derived from the equation, $B/L = 0.5n$. For B equal to 5 and 10 m, the frequencies corresponding to Eq. (4.2) for $n = 1$

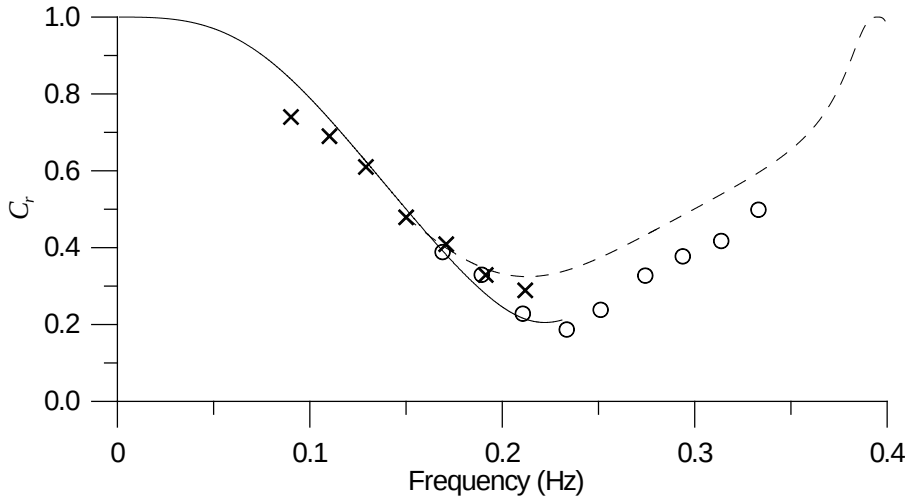

Fig. 4.7. Measured and calculated reflection coefficients (Porosity = 0.148, Wave chamber width = 5 m) : — = Calculation (Spectrum A), −− = Calculation (Spectrum B), x = Measurement (Spectrum A), ○ = Measurement (Spectrum B)

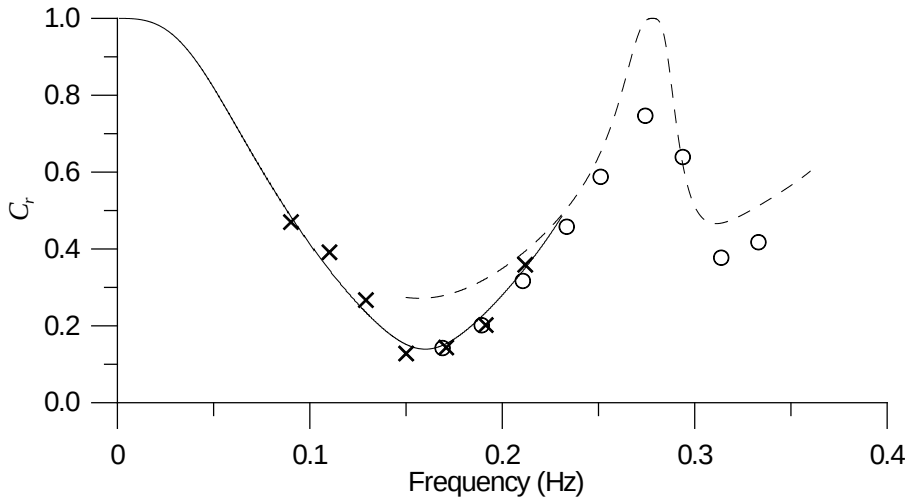

Fig. 4.8. Measured and calculated reflection coefficients (Porosity = 0.148, Wave chamber width = 10 m) : — = Calculation (Spectrum A), −− = Calculation (Spectrum B), x = Measurement (Spectrum A), ○ = Measurement (Spectrum B)

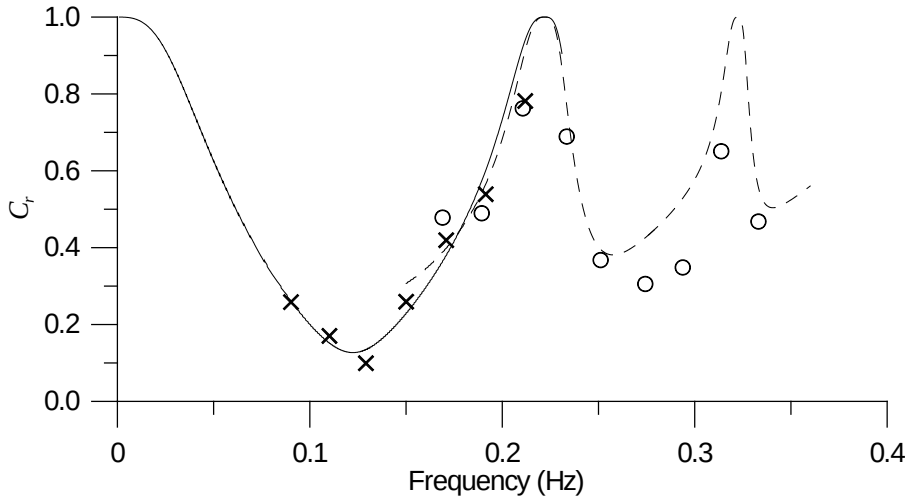

Fig. 4.9. Measured and calculated reflection coefficients (Porosity = 0.148, Wave chamber width = 15 m) : — = Calculation (Spectrum A), −− = Calculation (Spectrum B), x = Measurement (Spectrum A), ○ = Measurement (Spectrum B)

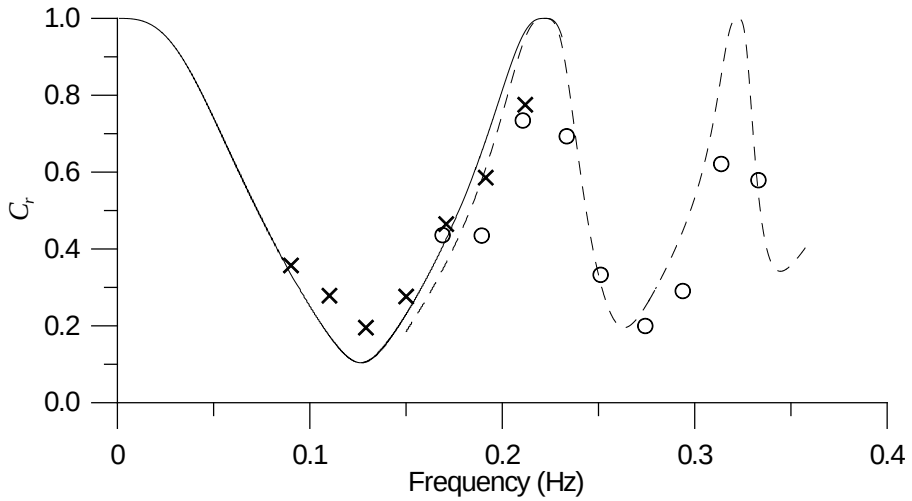

Fig. 4.10. Measured and calculated reflection coefficients (Porosity = 0.209, Wave chamber width = 15 m) : — = Calculation (Spectrum A), −− = Calculation (Spectrum B), x = Measurement (Spectrum A), ○ = Measurement (Spectrum B)

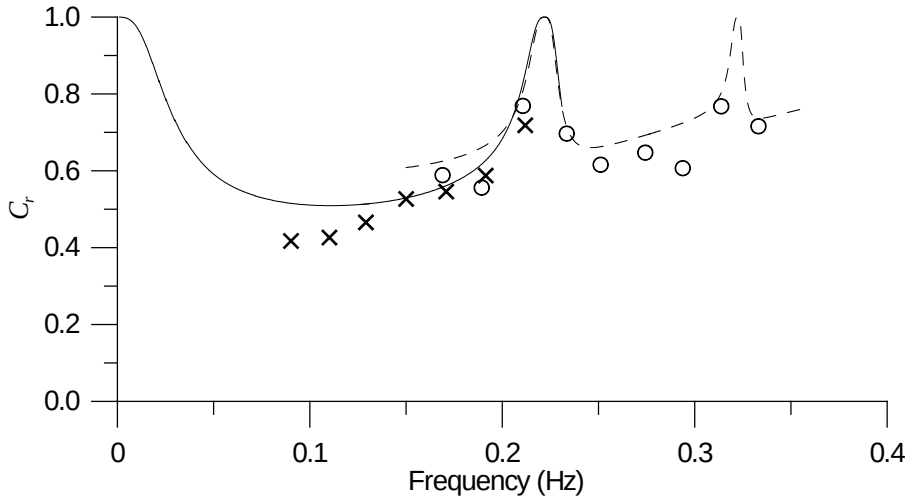

Fig. 4.11. Measured and calculated reflection coefficients (Porosity = 0.072, Wave chamber width = 15 m) : — = Calculation (Spectrum A), −− = Calculation (Spectrum B), x = Measurement (Spectrum A), ○ = Measurement (Spectrum B)

are 0.4 and 0.28 Hz, respectively. And for $B = 15\,\mathrm{m}$, it is 0.22 Hz. This means that, as the front perforated wall is located far from the backing wall, the peak reflection point of the curve moves toward the lower frequency. In the mean time, Figs. 4.9, 4.10 and 4.11 show comparisons for a fixed wave chamber width but varying porosity. As the porosity decreases, the curves are more sharply peaked and the troughs are more flattened. Even with the sharply peaked curves the theoretical model performs well.

The frequency averaged reflection coefficients obtained by Eq. (2.13) are listed in Table 4.3. As mentioned previously, the model somewhat over-predicts the reflection coefficients in most cases. And in general the result of spectrum B has the lower accuracy than that of spectrum A

Table 4.3 The frequency averaged reflection coefficients of Bennett et al. (1992) experiments

Fig. No.	Chamber width (m)	porosity	Spectrum A			Spectrum B		
			Exp.	Theory	Error(%)	Exp.	Theory	Error(%)
4.7	5	0.148	0.558	0.586	4.7	0.289	0.377	23.2
4.8	10	0.148	0.307	0.301	−1.9	0.443	0.532	16.8
4.9	15	0.148	0.366	0.394	7.1	0.569	0.646	11.9
4.10	15	0.209	0.415	0.434	4.3	0.542	0.671	19.3
4.11	15	0.072	0.511	0.566	9.8	0.657	0.708	7.2

CHAPTER 5

CONCLUDING REMARKS

5.1 Conclusions

Analytical models that can predict the reflection of regular or irregular waves from a perforated-wall caisson breakwater have been developed. Though such irregular wave models as Suh et al. (2001) become available, regular wave models are still in extensive use because of their simplicity. In the present study, using the regular wave model of Fugazza and Natale (1992), we calculated the reflection of irregular waves from a perforated-wall caisson breakwater in several different methods.

First, the regular wave model was re-validated by the hydraulic model tests. Laboratory experiments that involved regular waves of various wave heights and periods impinging upon breakwaters having various chamber widths were conducted. The model somewhat over-predicted the reflection coefficients at larger values and under-predicted them at smaller values because the model neglects the evanescent waves near the slits. But, overall agreement was pretty good. The reflection of waves is minimized when B/L is approximately 0.2, which is somewhat smaller than the theoretical value of 0.25 probably because of the effect of inertial resistance.

Then, using the regular wave model, the irregular wave reflection coefficients were calculated. In this study, the experimental results of Suh et al. (2001) and Bennett et al. (1992) were used. In applying the regular wave model to irregular wave reflection, several different methods were adopted. One is to assume the irregular waves as a regular wave whose height and period are the same as the root-mean-squared wave height and significant wave period, respectively, of the irregular waves (Method 1). Another way is to use the regular wave model repeatedly for each frequency component of the irregular waves (Method 2). The comparison between measurement and calculation has shown that the model using the Method 1 considerably over-predicts the reflection coefficients at larger values, while largely under-predicting them at smaller values. It was shown that the result calculated by Method 2 using the root-mean-squared wave height for all the frequencies gives fairly good agreement with the experimental data. However, the results of Method 2 using the wave height corresponding to the energy of each frequency component severely over-predicted the reflection coefficients.

Based on the facts that have been clarified so far, the following conclusions can be drawn. It is the most reasonable to use the regular wave model repeatedly for each frequency component of the irregular waves by assuming the wave height of irregular waves as the root-mean-squared wave height for all the frequencies.

5.2 Future studies

In the present study, we calculated the irregular wave reflection from a perforated-wall caisson breakwater using a regular wave model. However, even in the most error-free case, the model somewhat over-predicted the reflection coefficients at larger values, and under-predicted at smaller values. Hence, the modified model that can consider the evanescent waves near the breakwater may correct this problem.

And it may be meaningful to extend this theory to the case of the partially perforated-wall caisson mounted on a rubble mound. It is also necessary to develop the regular wave model which can predict the irregular wave reflection when the waves are obliquely incident to the breakwater. This remains a subject of future study.

REFERENCES

Bennett, G.S., McIver, P., Smallman, J.V., 1992. A mathematical model of slotted wavescreen breakwater. *Coastal Eng.*, 18: 231-249.

Fugazza, M., Natale, L., 1992. Hydraulic design of perforated breakwaters. *J. Waterw. Port Coastal Ocean Eng.*, 118: 1-14.

Goda, Y., 2000. *Random Seas and Design of Maritime Structures*. 2nd ed., World Scientific, Singapore, 443 pp.

Ijima, T., Okuzono, H. and Ushifusa, Y., 1978. The reflection coefficients of permeable quaywall with reservoir against obliquely incident waves. *Rep. Coll. Eng*., Kyushu Univ., 51: 243-250 (in Japanese).

Isaacson, M., Baldwin, J., Allyn, N., Cowdell, S., 2000. Wave interactions with perforated breakwaters. *J. Waterw. Port Coastal Ocean Eng.*, 126(5): 229-235.

Isaacson, M., Baldwin, J., Premasiri, G., Yang, G., 1999. Wave interactions with double slotted barriers. *Appl. Ocean Res*., 21, 81-91.

Isaacson, M., Premasir, S., Yang, G., 1998. Wave interactions with vertical slotted barrier. *J. Waterw. Port Coastal Ocean Eng.* 124(3): 118-126.

Jarlan, G.E., 1961. A perforated vertical wall breakwater. *Dock Harbour Auth.*, XII(486): 394-398.

Kakuno, S., Liu, P.L.-F., 1993. Scattering of water waves by vertical cylinders.

J. Waterw. Port Coastal Ocean Eng., 119: 302-322.

Kakuno, S., Nakata, Y., 1998. Scattering of water waves by rows of cylinders with/without a backwall. . *Appl. Ocean Res.*, 20: 191-198.

Kakuno, S., Oda, K., Liu, P.L.-F., 1992. Scattering of water waves by vertical cylinders with a backwall. In: *Proc. 23rd Coastal Eng. Conf.*, Venice, Vol. 2, pp. 1258-1271.

Kondo, H., 1979. Analysis of breakwaters having two porous walls. In: *Proc. Coastal Structures '79*, Vol. 2, pp. 962-977.

Marks, M., Jarlan, G.E., 1968. Experimental study on a fixed perforated breakwater. In: *Proc. 11th Coastal Eng. Conf., London*, Vol. 3, pp. 1121-1140.

Mei, C.C., Liu, P.L.-F., Ippen, A.T., 1974. Quadratic loss and scattering of long waves. *J. Waterways, Harbors Coastal Eng. Div.,* ASCE, 100: 217-239.

Messel, S. R., 1993. Extended refraction-diffraction equation for surface waves. *Coastal Eng.*, 19: 97-126.

Park, W.S., Chun, I.S., Lee, D.S., 1993. Hydraulic experiments for the reflection characteristics of perforated breakwaters. *J. Korean Soc. Coastal Ocean Engrs.* 5: 198-203 (in Korean, with English abstract).

Park, W.S., Kim, B.H., Suh, K.D., Lee, K.S., 2000. Scattering of irregular waves by vertical cylinders. *Coastal Eng. J.*, 42: 253-271.

Park, W.S., Oh, Y.M., Chun, I.S., 1992. Separation technique of incident and

reflected waves using least squares method. *J. Korean Soc. Coastal Ocean Engrs*. 4: 139-145 (in Korean, with English abstract).

Suh, K.D., 1996. Wave reflection form partially perforated caisson breakwater. *J. Korean Soc. Coastal Ocean Engrs.* 8(3): 221-230.

Suh, K.D., Choi, J.C., Kim, B.H., Park, W.S., Lee, K.S., 2001. Reflection of irregular waves from perforated-wall caisson breakwaters. *Coastal Eng.* 44: 141-151.

Suh, K.D., Park, W.S., 1995. Wave reflection from perforated-wall caisson breakwaters. *Coastal Eng.*, 26: 177-193.

Takahashi, S., Shimosako, K., 1994. Wave pressure on a perforated caisson. In: *Proc. Hydro-Port'94. Port and Harbour Res. Inst.*, Yokosuka, Vol. 1, pp. 747-764.

Takahashi, S., Tanimoto, K., Shimosako, K., 1994. A proposal of impulsive pressure coefficient for the design of composite breakwaters. In: *Proc. Hydro-Port'94. Port and Harbour Res. Inst.*, Yokosuka, Vol. 1, pp. 489-504.

Tanimoto, K., Haranaka, S., Takahashi, S., Komatsu, K., Todoroki, M., Osato, M., 1976. An experimental investigation of wave reflection, overtopping and wave forces for several types of breakwaters and sea walls. *Tech. Note of Port and Harbour Res. Inst.*, Ministry of Transport, Japan, No. 246, 38 pp. (in Japanese, with English abstract).

Terret, F.L., Osorio, J.D.C., Lean, G.H., 1968. Model studies of a perforated

breakwater. In: *Proc. 11th Coastal Eng. Conf.*, London, Vol. 3, pp. 1104-1120.

Williams, N., Mansour, A.M., Lee, H.S., 2000. Simplified analytical solutions for wave interaction with absorbing-type caisson breakwaters. *Coastal Eng.*, 27: 1231-1248.

Willmott, C.J., 1981. On the validation of models. *Phys. Geog*. 2: 184-194.

APPENDICES

A. Comparison of measured and calculated spectra of incident and reflected waves

B. Photos of laboratory experiment

Appendix A. Comparison of measured and calculated spectra of incident and reflected waves

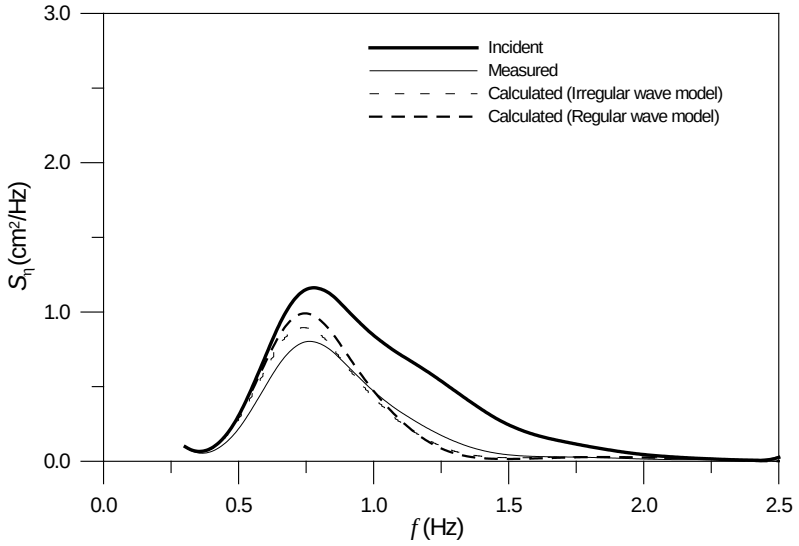

Fig. A.1. Measured and calculated spectra of incident and reflected waves ($H_s \cong 3$ cm, $T_s \cong 1.0$ s, B = 15 cm)

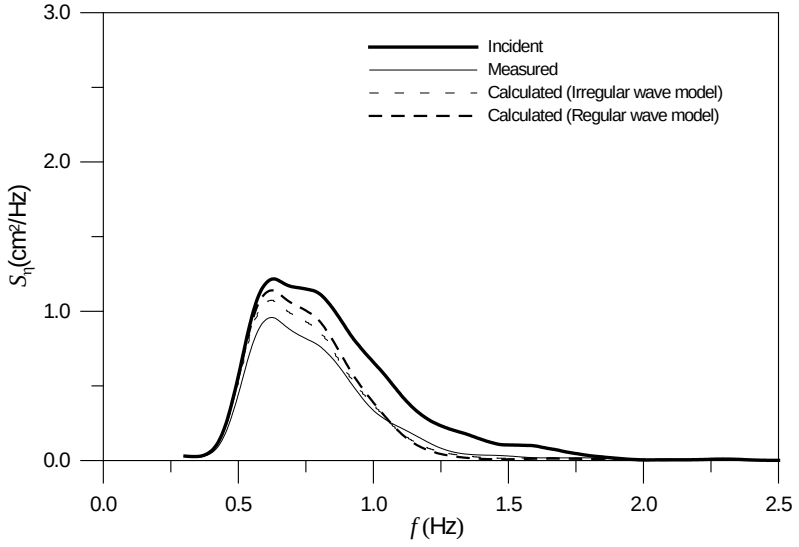

Fig. A.2. Measured and calculated spectra of incident and reflected waves ($H_s \cong 3$ cm, $T_s \cong 1.2$ s, B = 15 cm)

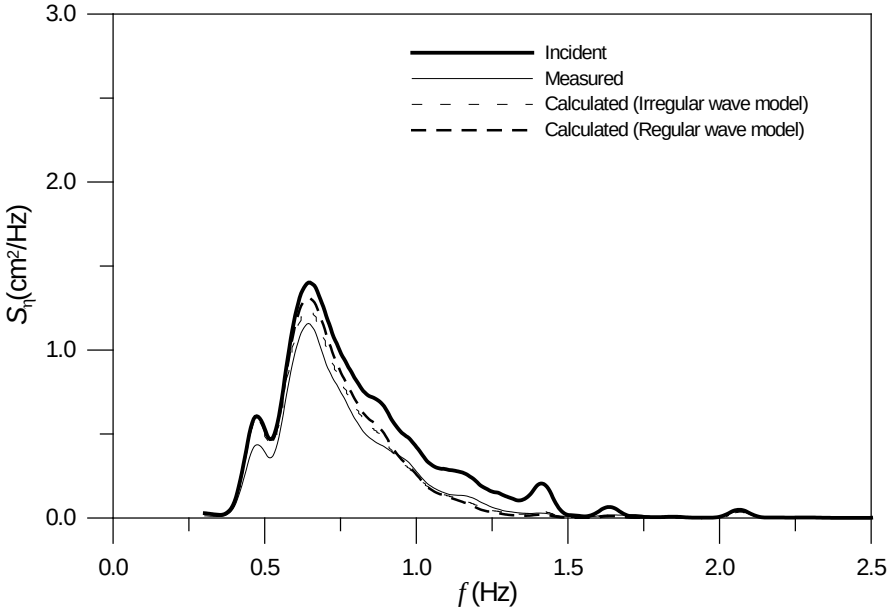

Fig. A.3. Measured and calculated spectra of incident and reflected waves ($H_s \cong 3$ cm, $T_s \cong 1.4$ s, B = 15 cm)

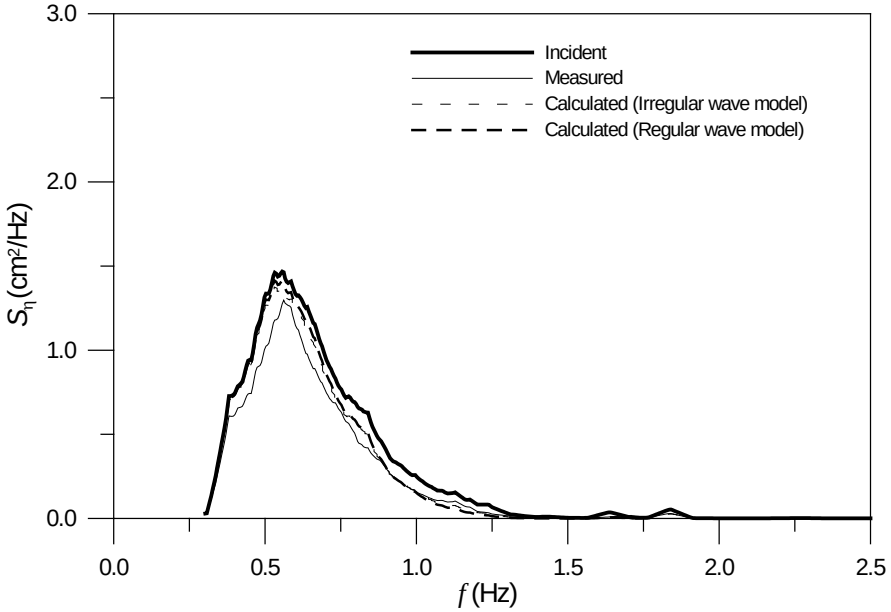

Fig. A.4. Measured and calculated spectra of incident and reflected waves ($H_s \cong 3$ cm, $T_s \cong 1.6$ s, B = 15 cm)

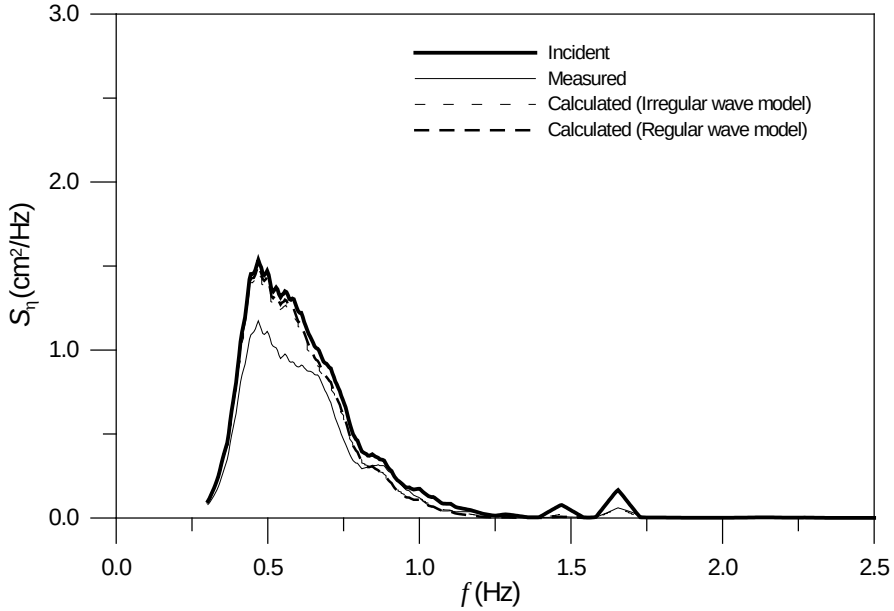

Fig. A.5. Measured and calculated spectra of incident and reflected waves ($H_s \cong 3$ cm, $T_s \cong 1.8$ s, B = 15 cm)

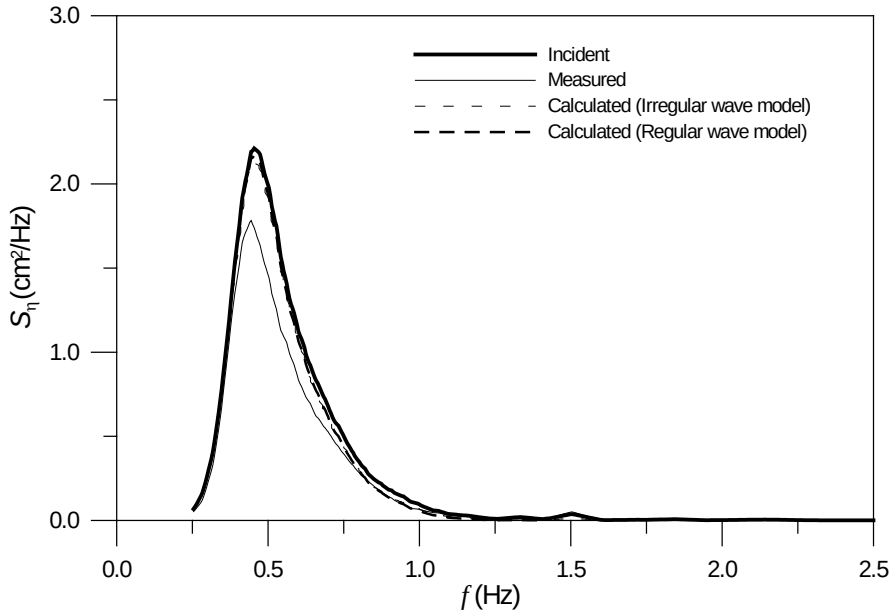

Fig. A.6. Measured and calculated spectra of incident and reflected waves ($H_s \cong 3$ cm, $T_s \cong 2.0$ s, B = 15 cm)

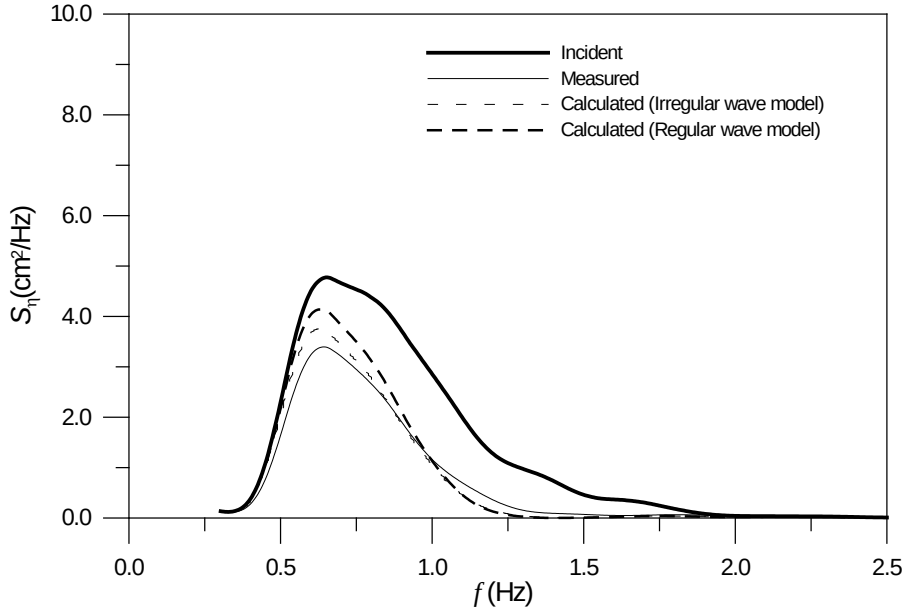

Fig. A.7. Measured and calculated spectra of incident and reflected waves ($H_s \cong 6$ cm, $T_s \cong 1.2$ s, B = 15 cm)

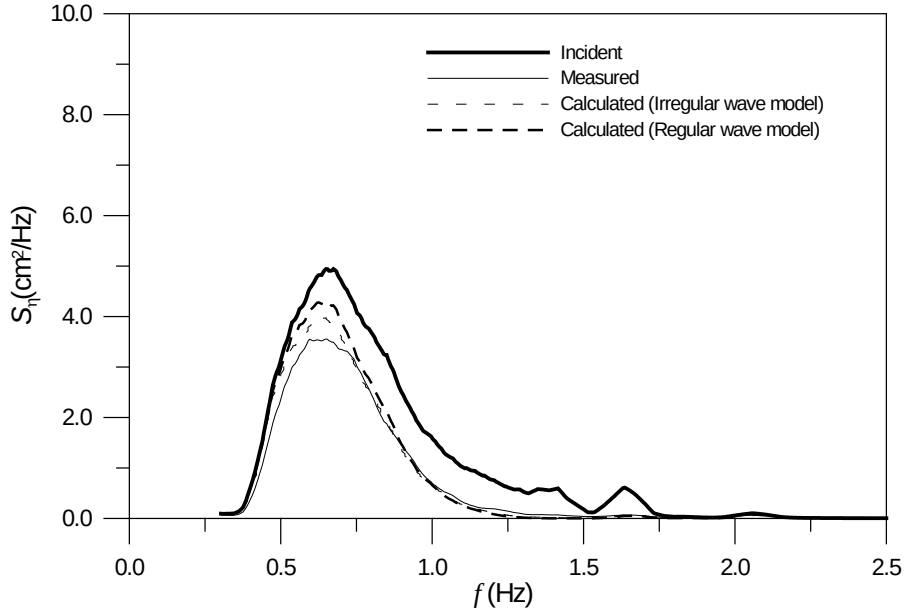

Fig. A.8. Measured and calculated spectra of incident and reflected waves ($H_s \cong 6$ cm, $T_s \cong 1.4$ s, B = 15 cm)

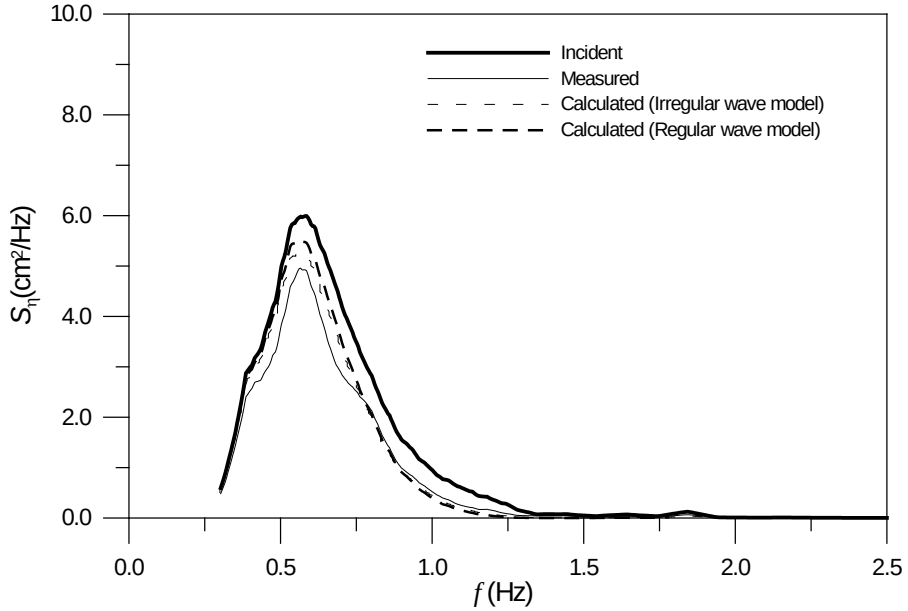

Fig. A.9. Measured and calculated spectra of incident and reflected waves ($H_s \cong 6$ cm, $T_s \cong 1.6$ s, B = 15 cm)

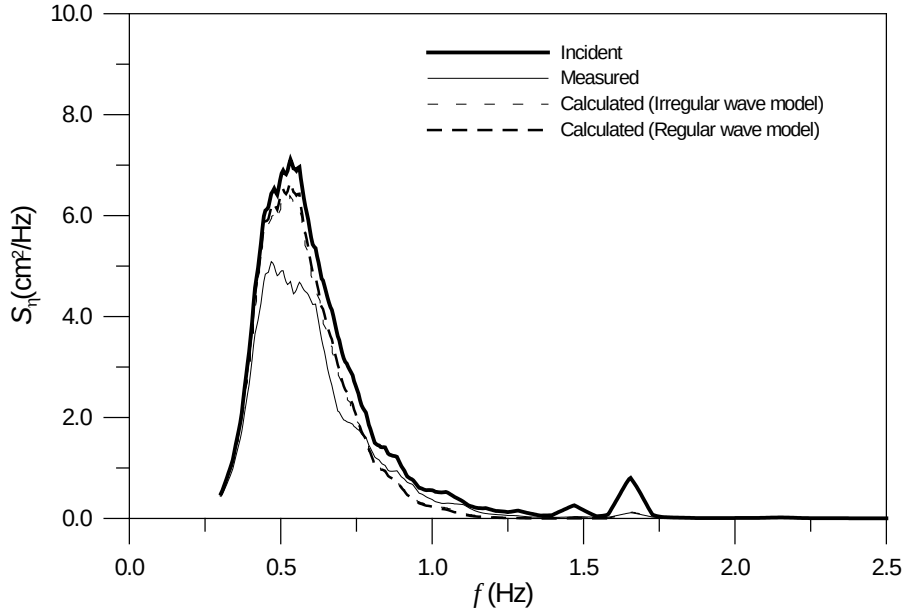

Fig. A.10. Measured and calculated spectra of incident and reflected waves ($H_s \cong 6$ cm, $T_s \cong 1.8$ s, B = 15 cm)

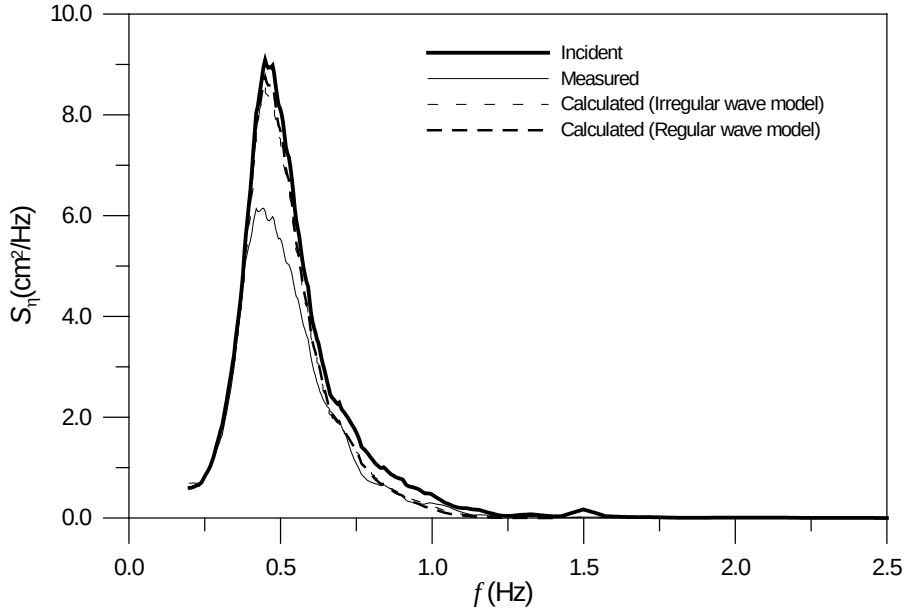

Fig. A.11. Measured and calculated spectra of incident and reflected waves ($H_s \cong 6$ cm, $T_s \cong 2.0$ s, $B = 15$ cm)

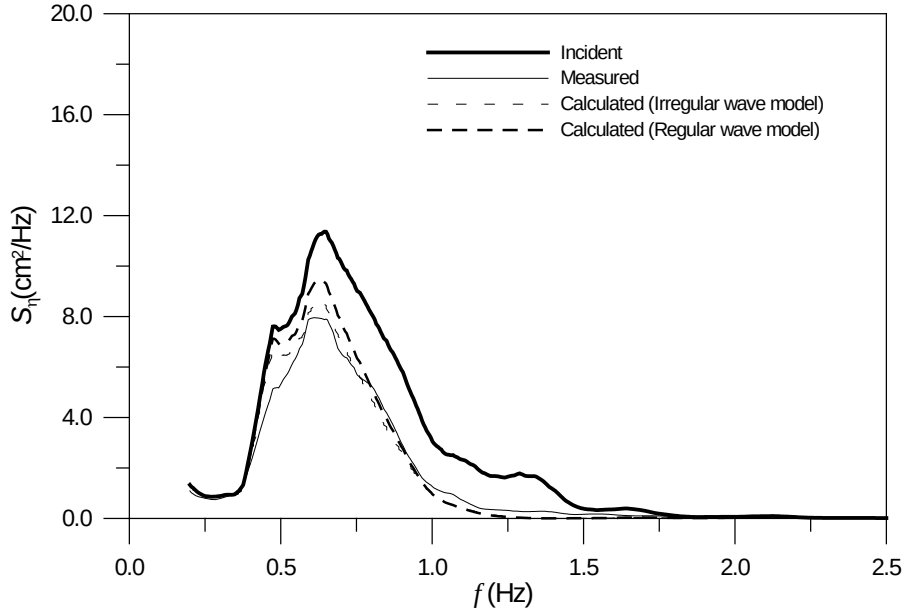

Fig. A.12. Measured and calculated spectra of incident and reflected waves ($H_s \cong 9$ cm, $T_s \cong 1.4$ s, $B = 15$ cm)

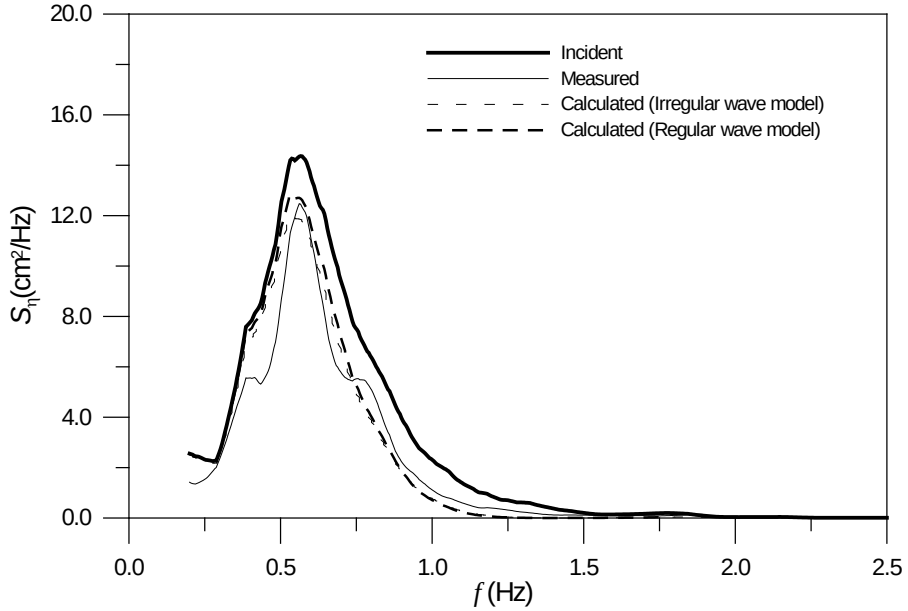

Fig. A.13. Measured and calculated spectra of incident and reflected waves ($H_s \cong 9$ cm, $T_s \cong 1.6$ s, B = 15 cm)

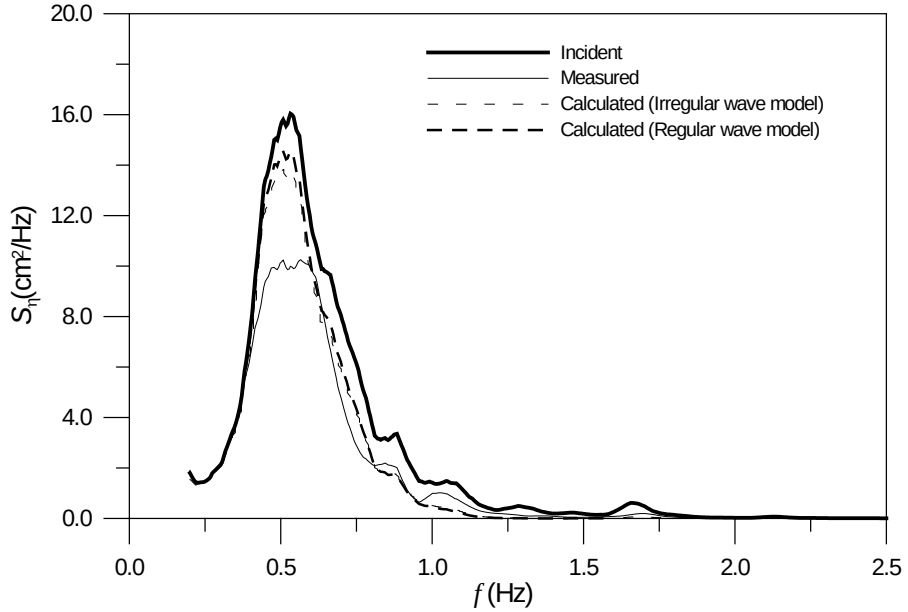

Fig. A.14. Measured and calculated spectra of incident and reflected waves ($H_s \cong 9$ cm, $T_s \cong 1.8$ s, B = 15 cm)

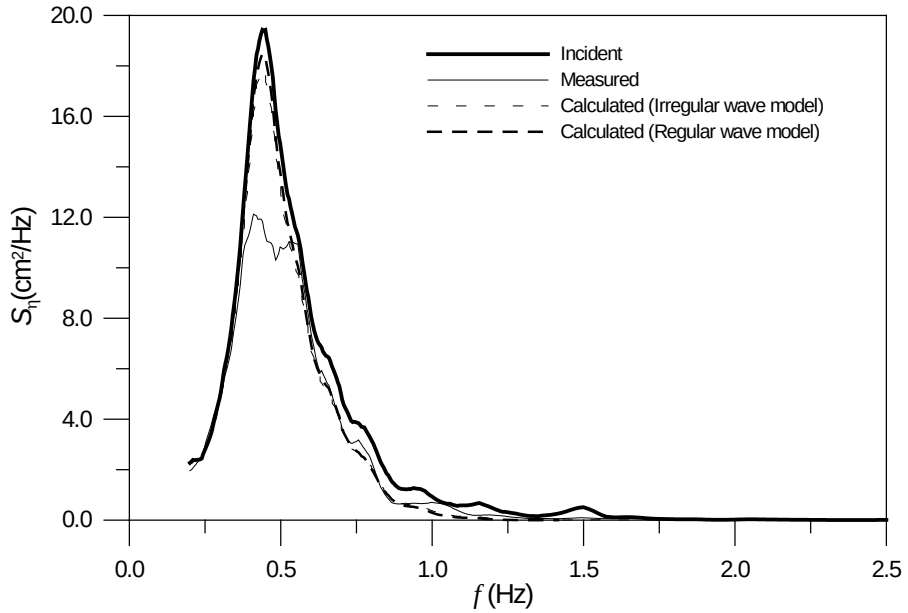

Fig. A.15. Measured and calculated spectra of incident and reflected waves ($H_s \cong 9$ cm, $T_s \cong 2.0$ s, $B = 15$ cm)

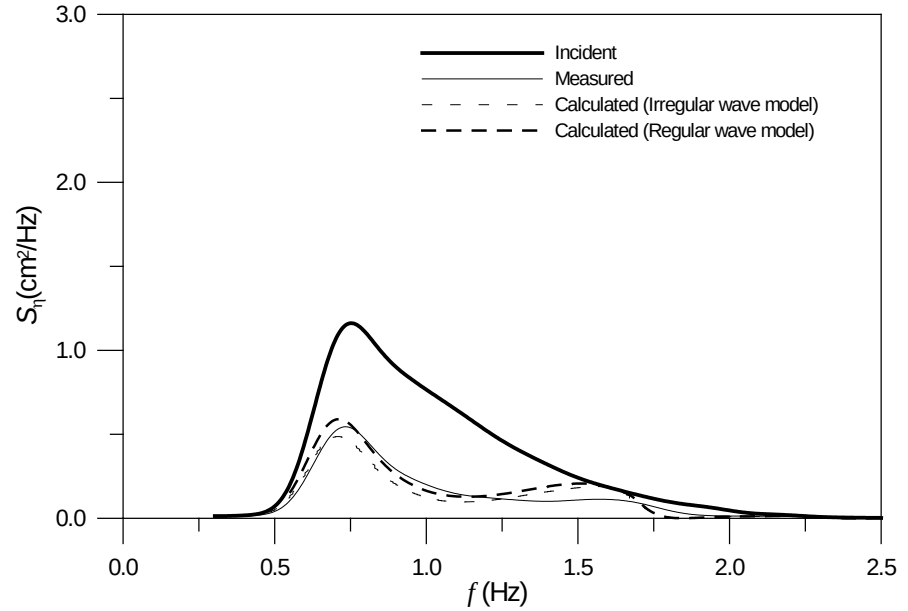

Fig. A.16. Measured and calculated spectra of incident and reflected waves ($H_s \cong 3$ cm, $T_s \cong 1.0$ s, $B = 30$ cm)

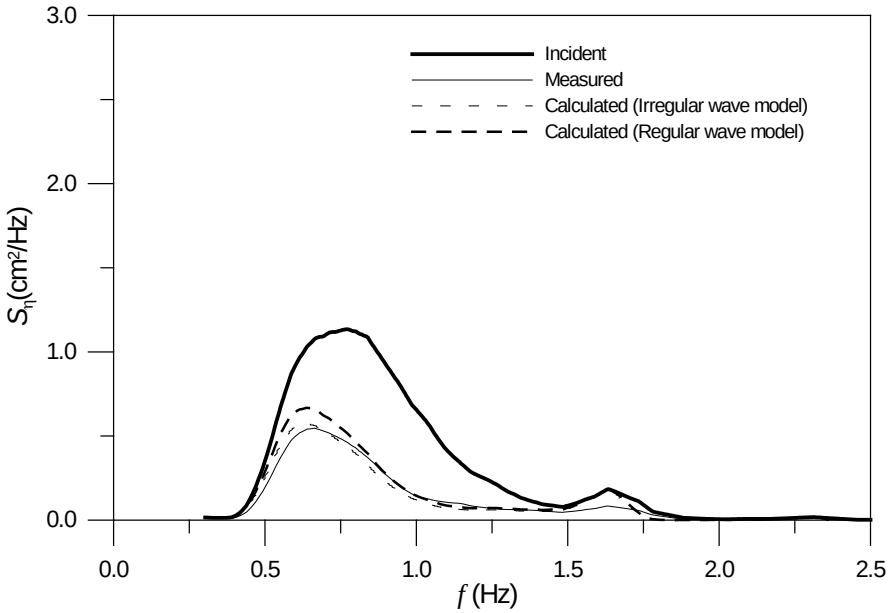

Fig. A.17. Measured and calculated spectra of incident and reflected waves ($H_s \cong 3$ cm, $T_s \cong 1.2$ s, B = 30 cm)

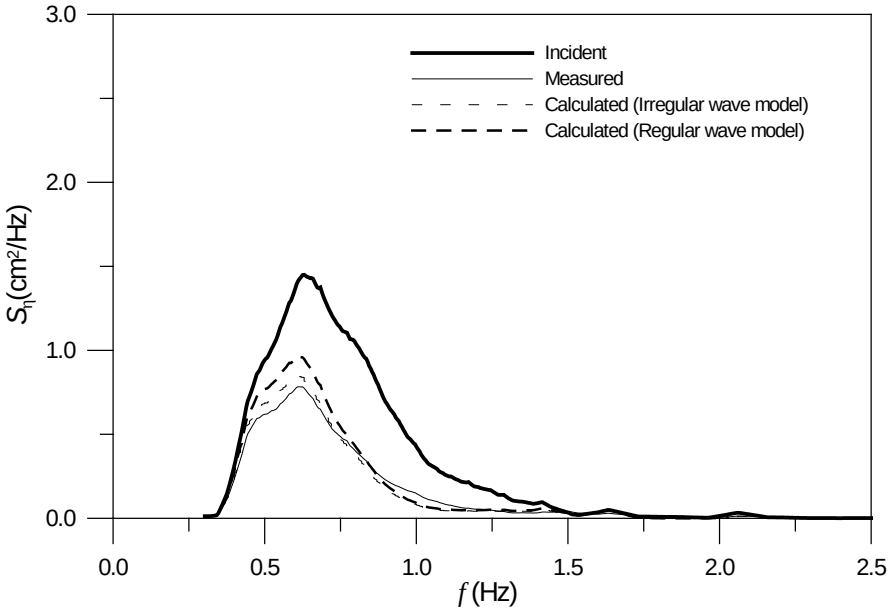

Fig. A.18. Measured and calculated spectra of incident and reflected waves ($H_s \cong 3$ cm, $T_s \cong 1.4$ s, B = 30 cm)

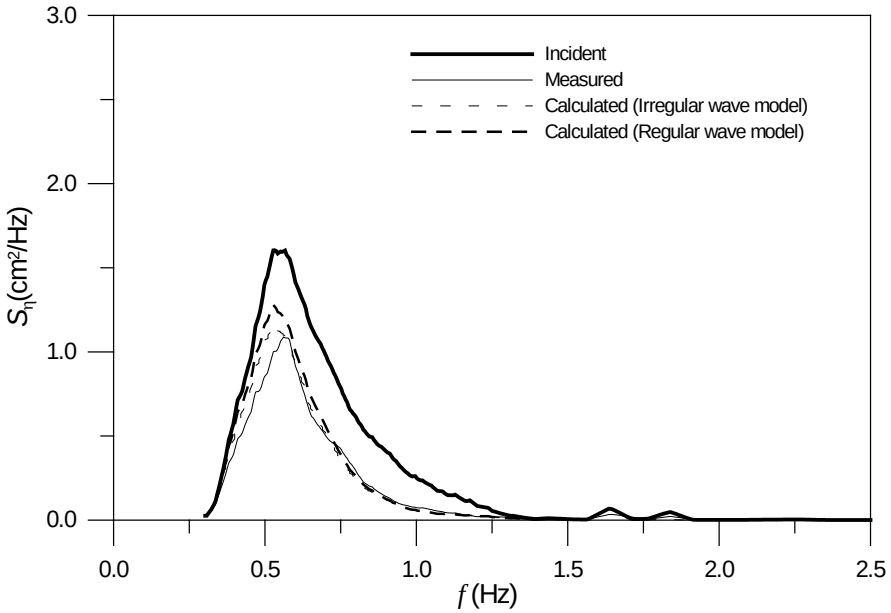

Fig. A.19. Measured and calculated spectra of incident and reflected waves ($H_s \cong 3$ cm, $T_s \cong 1.6$ s, B = 30 cm)

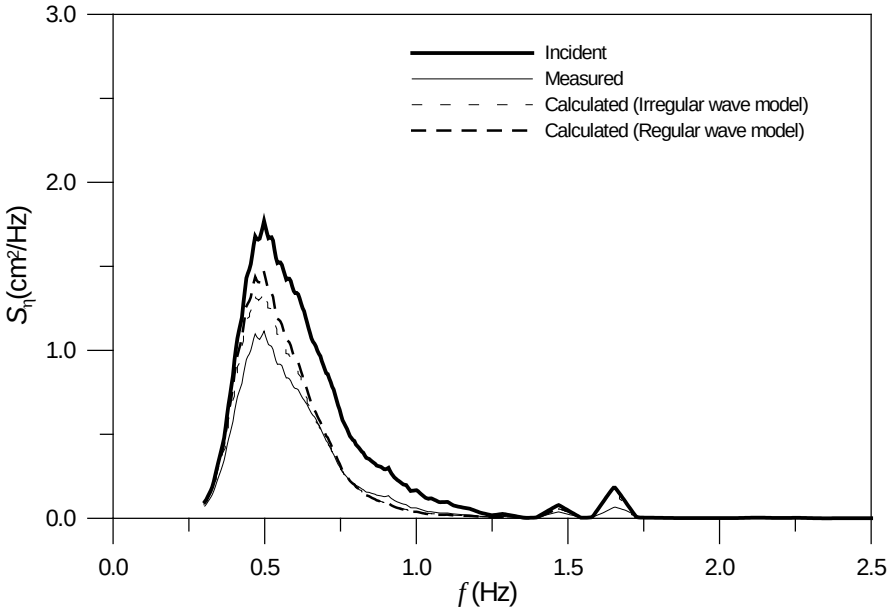

Fig. A.20. Measured and calculated spectra of incident and reflected waves ($H_s \cong 3$ cm, $T_s \cong 1.8$ s, B = 30 cm)

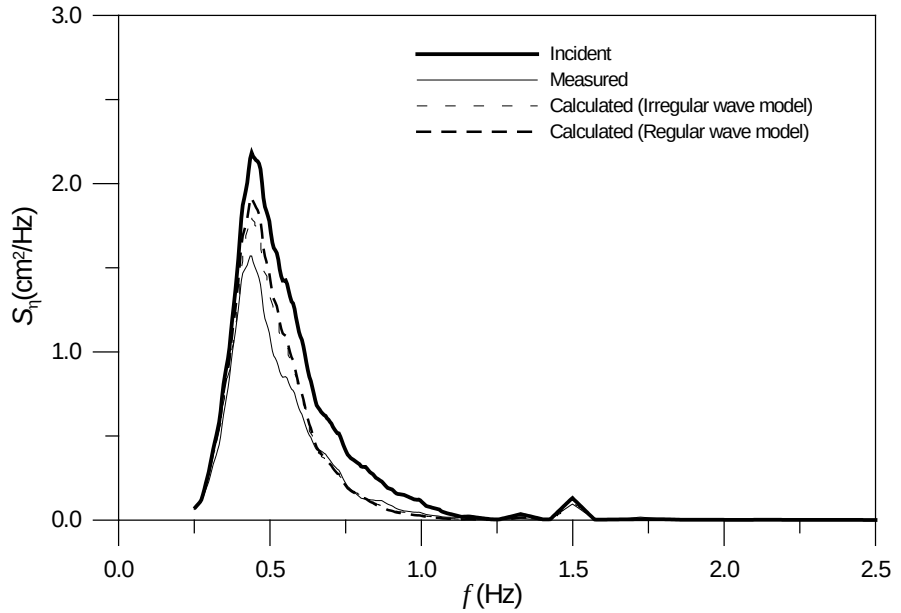

Fig. A.21. Measured and calculated spectra of incident and reflected waves ($H_s \cong 3$ cm, $T_s \cong 2.0$ s, $B = 30$ cm)

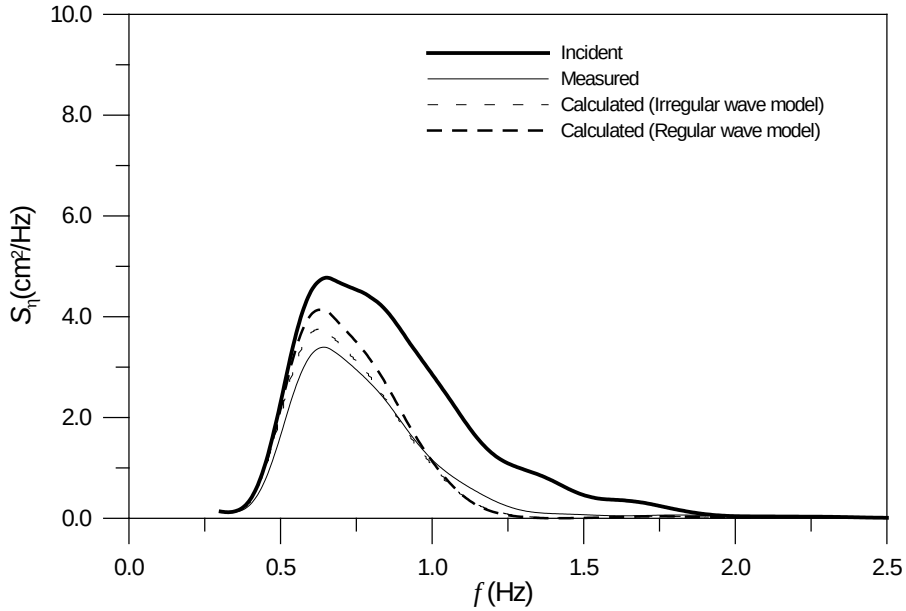

Fig. A.22. Measured and calculated spectra of incident and reflected waves ($H_s \cong 6$ cm, $T_s \cong 1.2$ s, $B = 30$ cm)

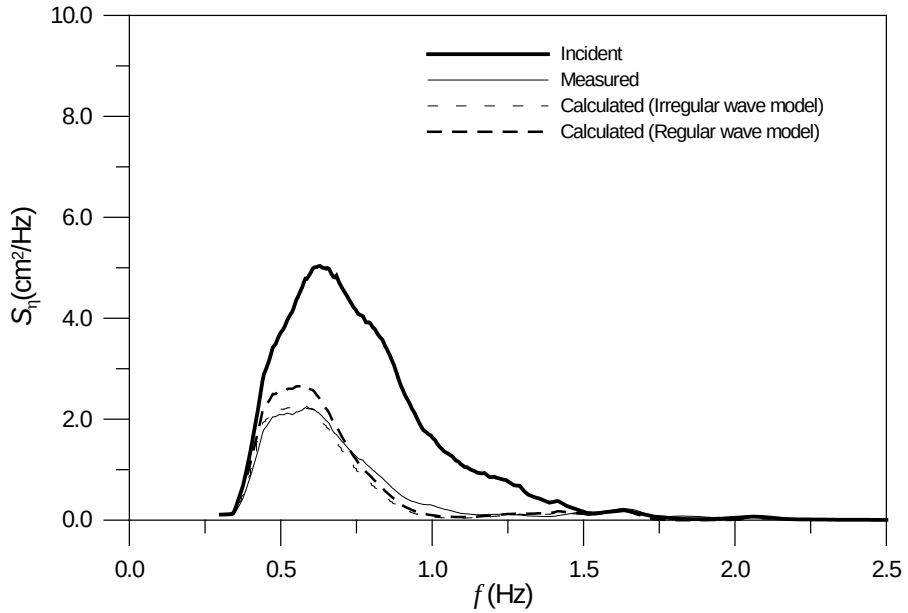

Fig. A.23. Measured and calculated spectra of incident and reflected waves ($H_s \cong 6$ cm, $T_s \cong 1.4$ s, $B = 30$ cm)

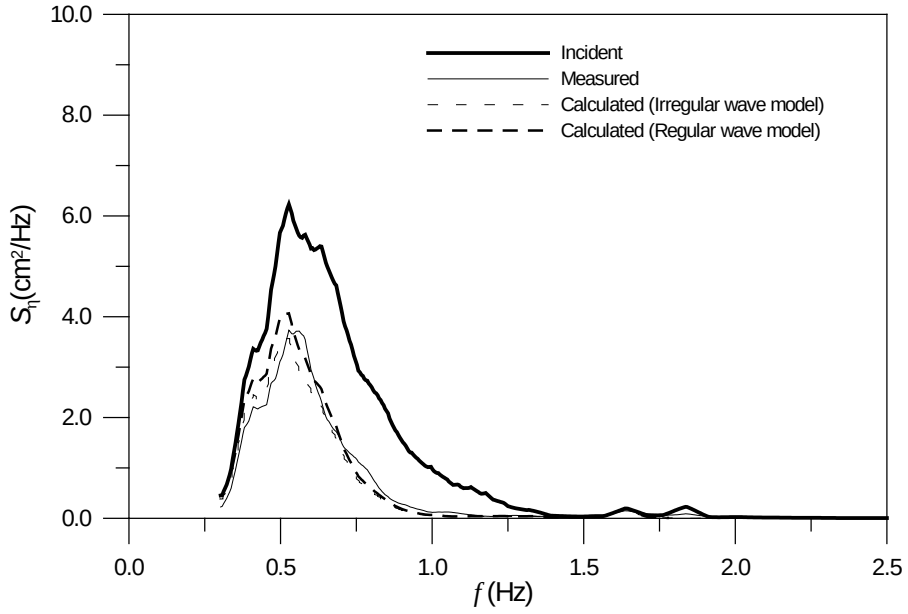

Fig. A.24. Measured and calculated spectra of incident and reflected waves ($H_s \cong 6$ cm, $T_s \cong 1.6$ s, $B = 30$ cm)

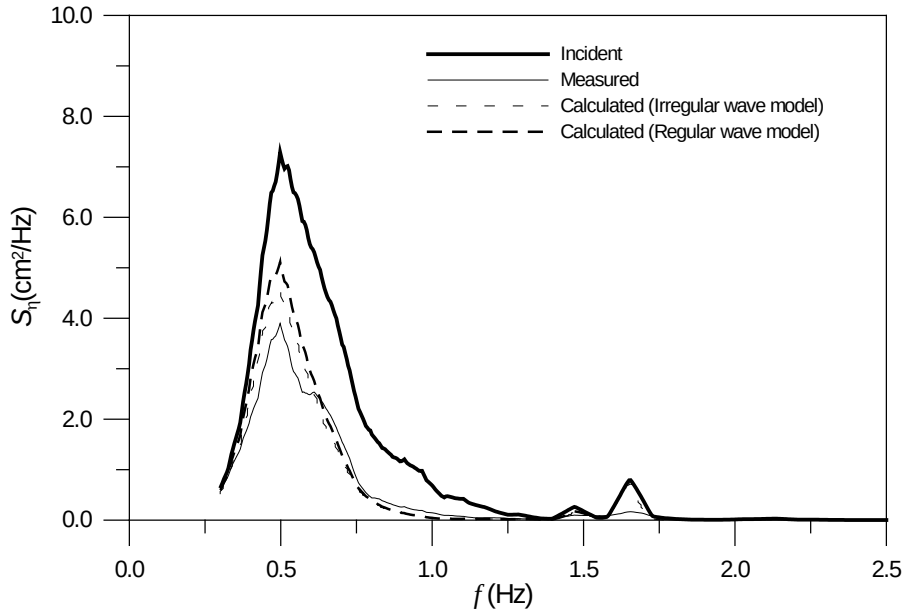

Fig. A.25. Measured and calculated spectra of incident and reflected waves ($H_s \cong 6$ cm, $T_s \cong 1.8$ s, $B = 30$ cm)

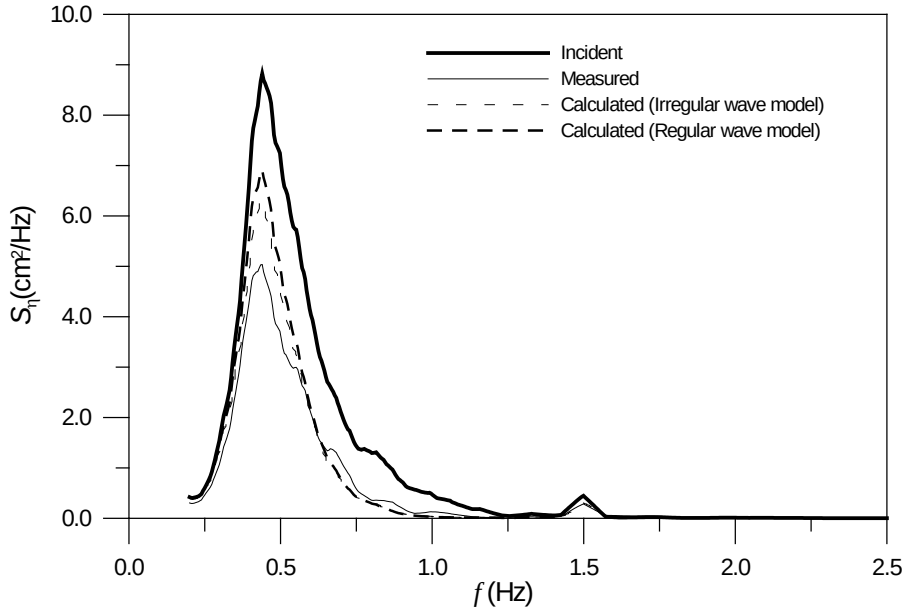

Fig. A.26. Measured and calculated spectra of incident and reflected waves ($H_s \cong 6$ cm, $T_s \cong 2.0$ s, $B = 30$ cm)

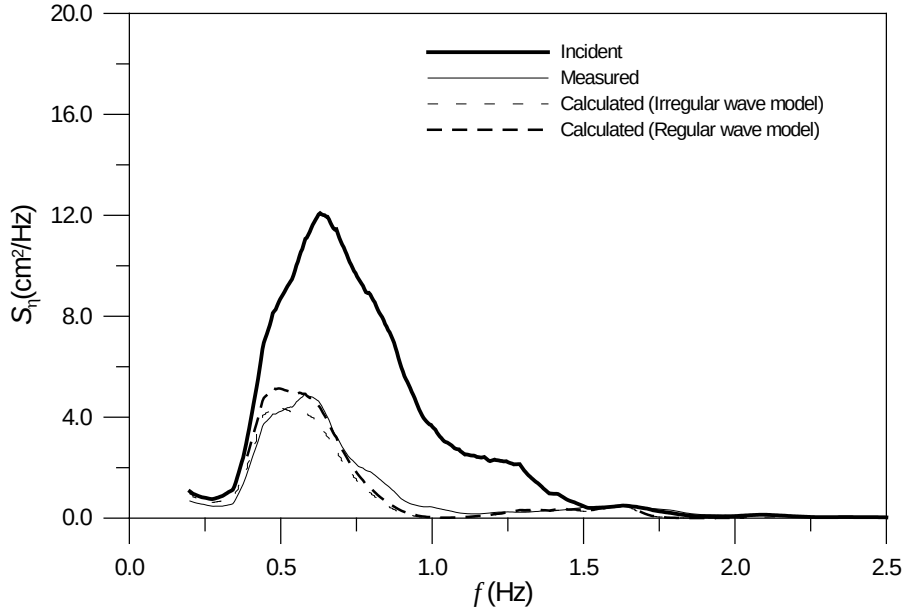

Fig. A.27. Measured and calculated spectra of incident and reflected waves ($H_s \cong 9$ cm, $T_s \cong 1.4$ s, B = 30 cm)

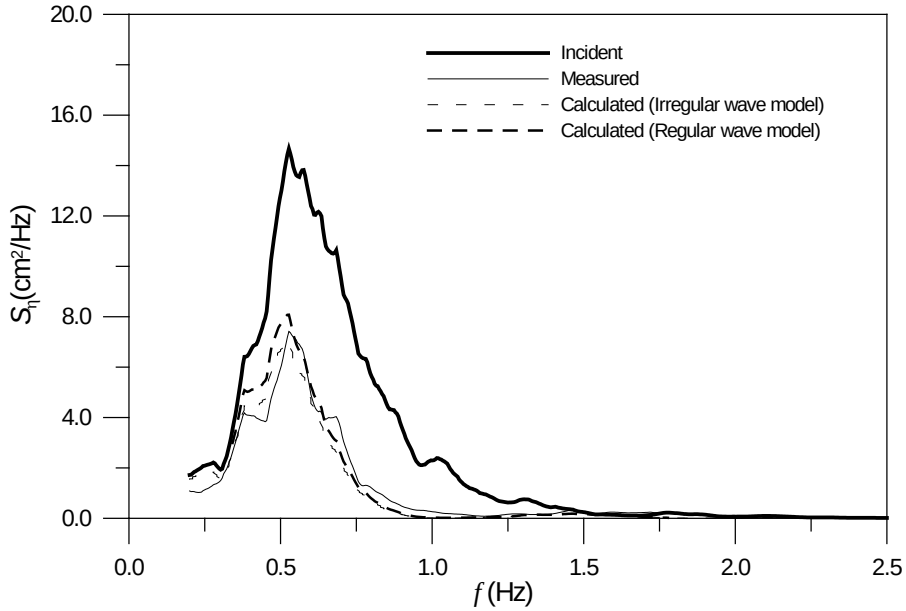

Fig. A.28. Measured and calculated spectra of incident and reflected waves ($H_s \cong 9$ cm, $T_s \cong 1.6$ s, B = 30 cm)

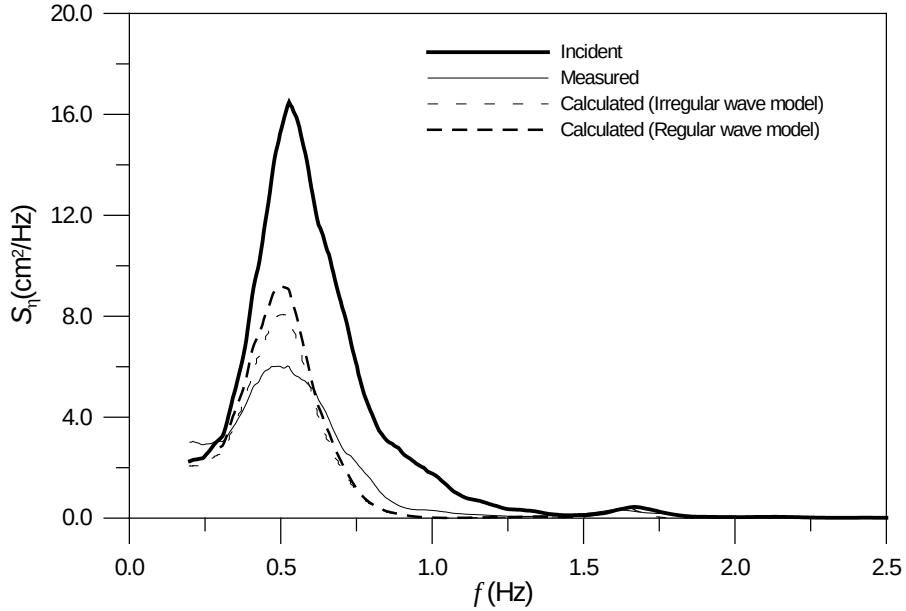

Fig. A.29. Measured and calculated spectra of incident and reflected waves ($H_s \cong 9$ cm, $T_s \cong 1.8$ s, $B = 30$ cm)

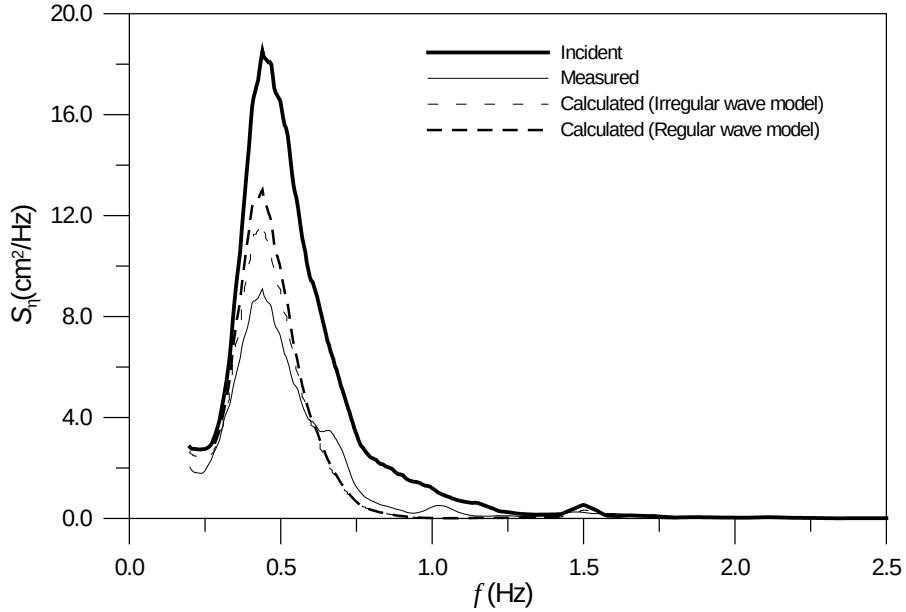

Fig. A.30. Measured and calculated spectra of incident and reflected waves ($H_s \cong 9$ cm, $T_s \cong 2.0$ s, $B = 30$ cm)

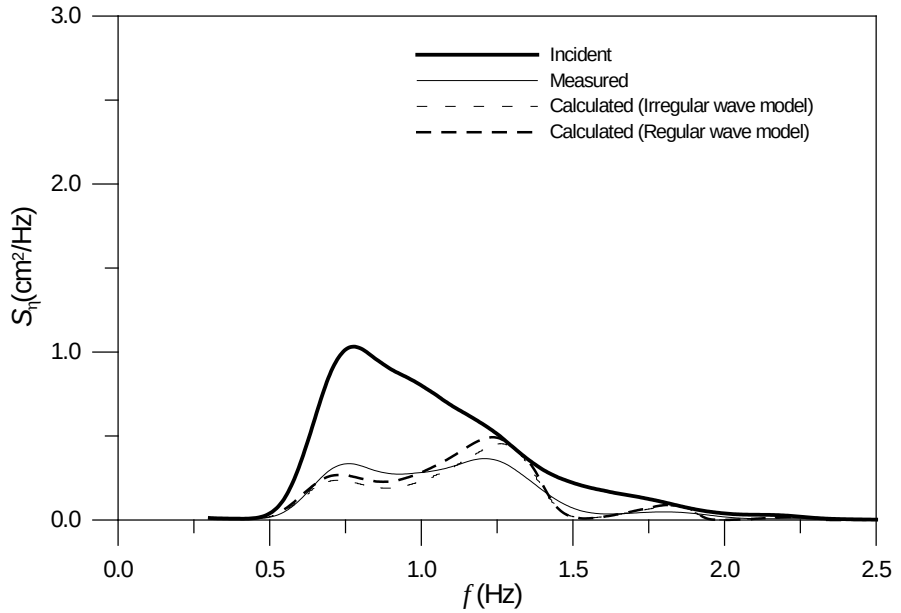

Fig. A.31. Measured and calculated spectra of incident and reflected waves ($H_s \cong 3$ cm, $T_s \cong 1.0$ s, $B = 45$ cm)

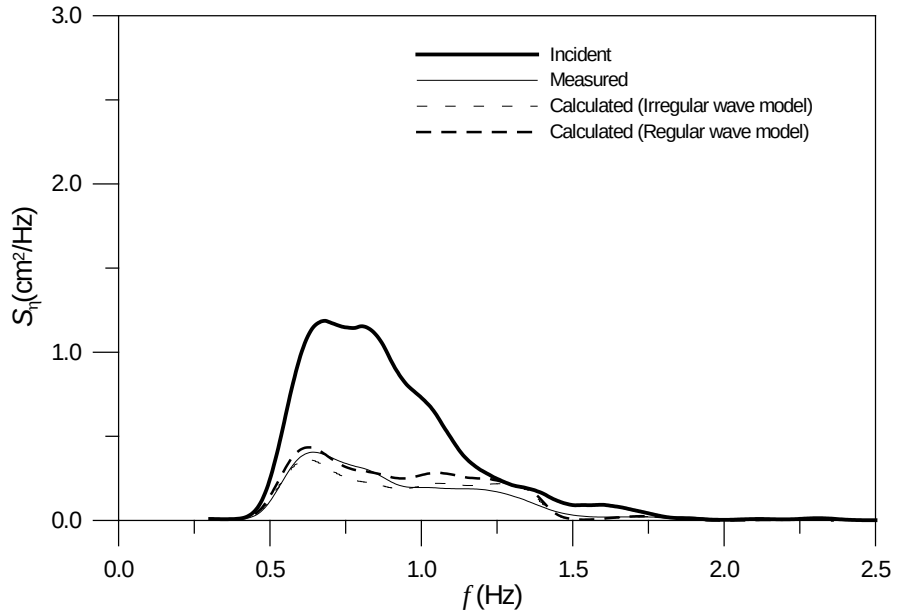

Fig. A.32. Measured and calculated spectra of incident and reflected waves ($H_s \cong 3$ cm, $T_s \cong 1.2$ s, $B = 45$ cm)

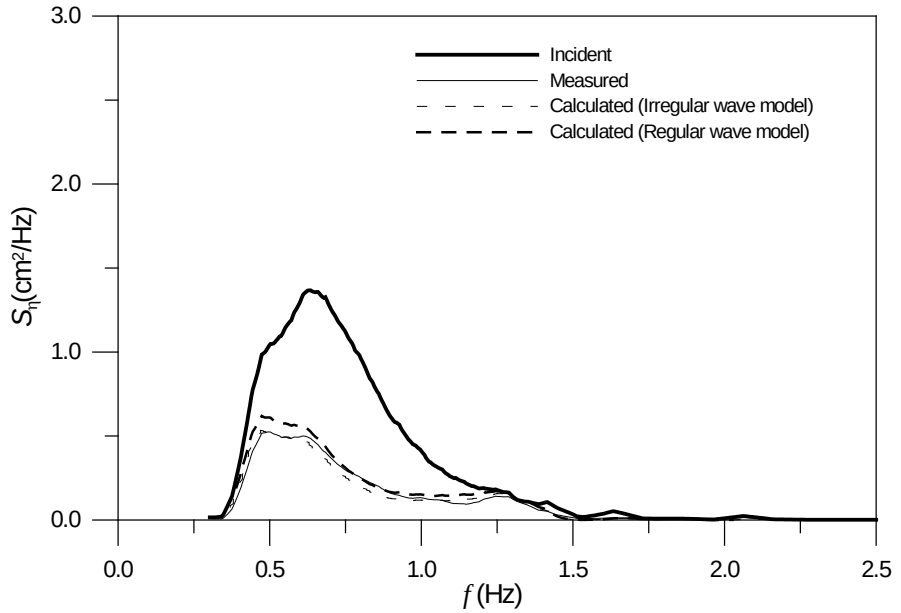

Fig. A.33. Measured and calculated spectra of incident and reflected waves ($H_s \cong 3$ cm, $T_s \cong 1.4$ s, $B = 45$ cm)

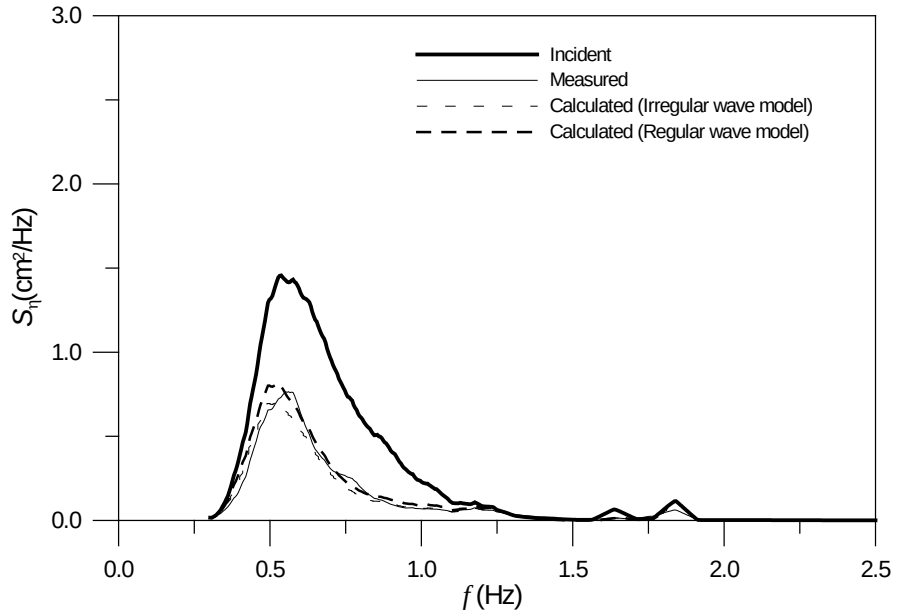

Fig. A.34. Measured and calculated spectra of incident and reflected waves ($H_s \cong 3$ cm, $T_s \cong 1.6$ s, $B = 45$ cm)

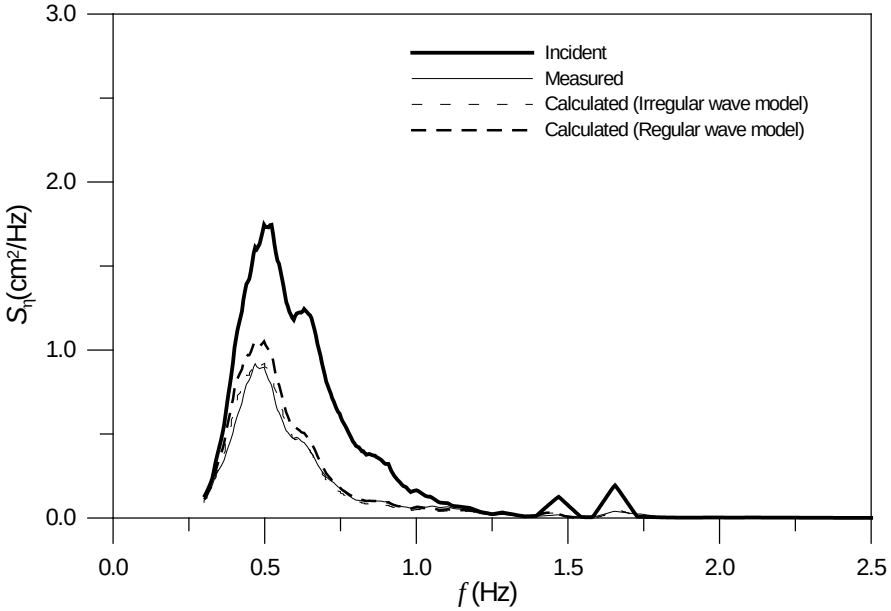

Fig. A.35. Measured and calculated spectra of incident and reflected waves ($H_s \cong 3$ cm, $T_s \cong 1.8$ s, B = 45 cm)

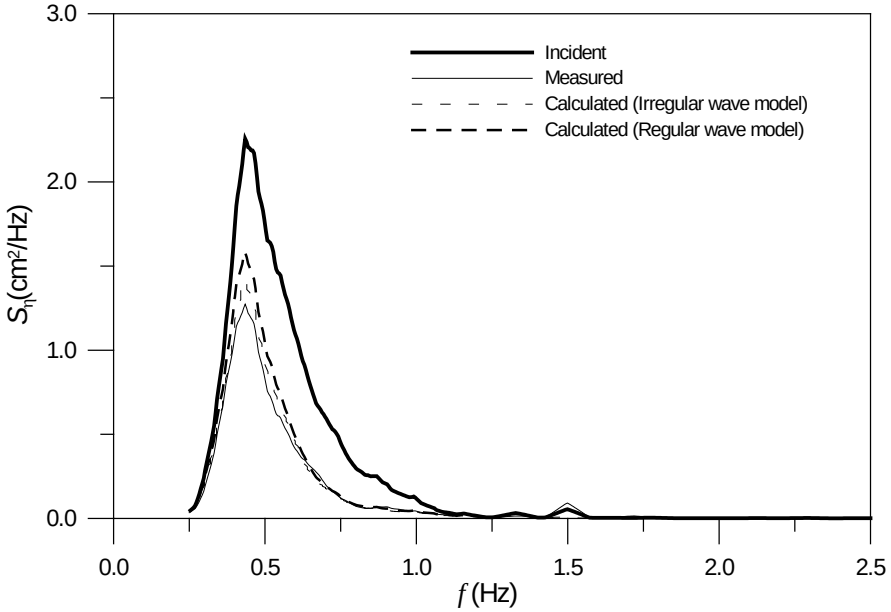

Fig. A.36. Measured and calculated spectra of incident and reflected waves ($H_s \cong 3$ cm, $T_s \cong 2.0$ s, B = 45 cm)

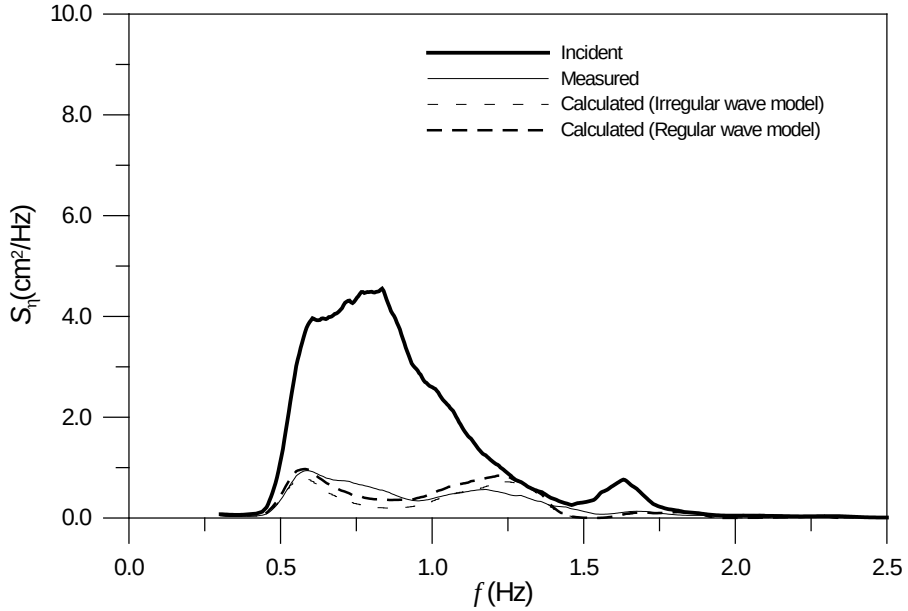

Fig. A.37. Measured and calculated spectra of incident and reflected waves ($H_s \cong 6$ cm, $T_s \cong 1.2$ s, $B = 45$ cm)

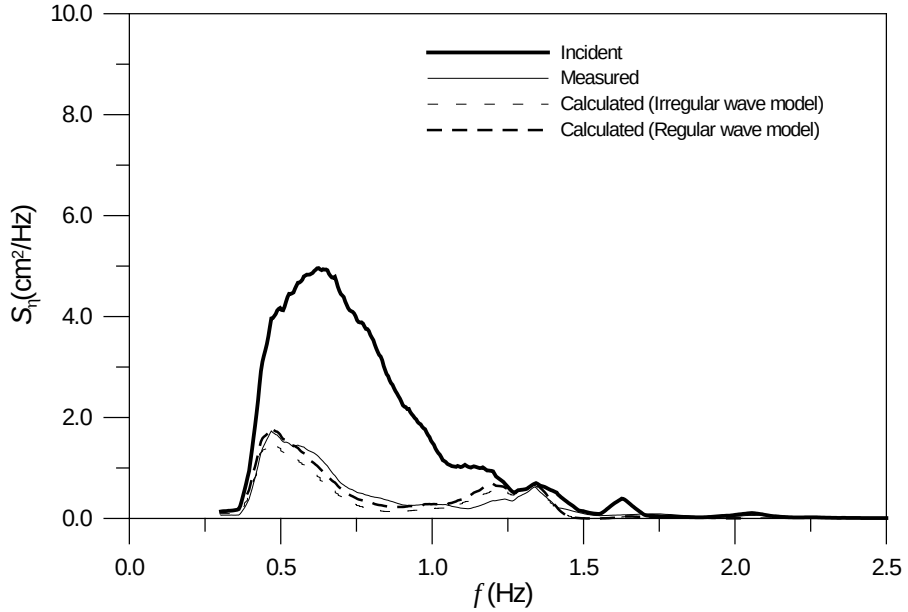

Fig. A.38. Measured and calculated spectra of incident and reflected waves ($H_s \cong 6$ cm, $T_s \cong 1.4$ s, $B = 45$ cm)

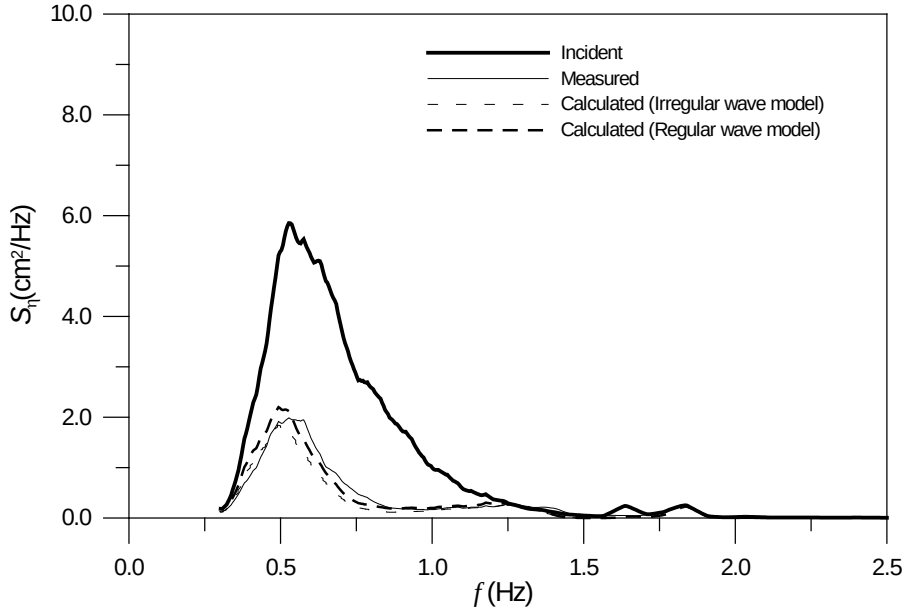

Fig. A.39. Measured and calculated spectra of incident and reflected waves ($H_s \cong 6$ cm, $T_s \cong 1.6$ s, $B = 45$ cm)

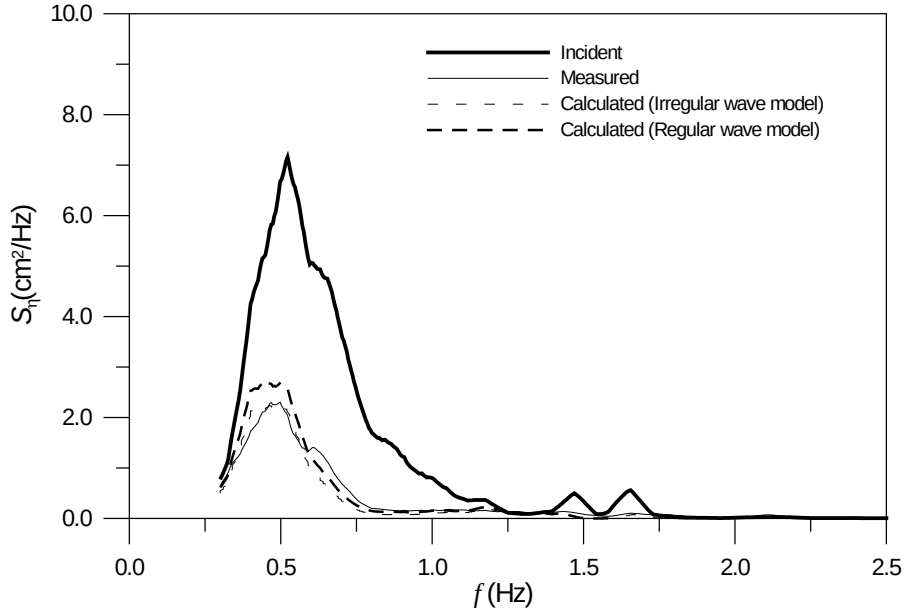

Fig. A.40. Measured and calculated spectra of incident and reflected waves ($H_s \cong 6$ cm, $T_s \cong 1.8$ s, $B = 45$ cm)

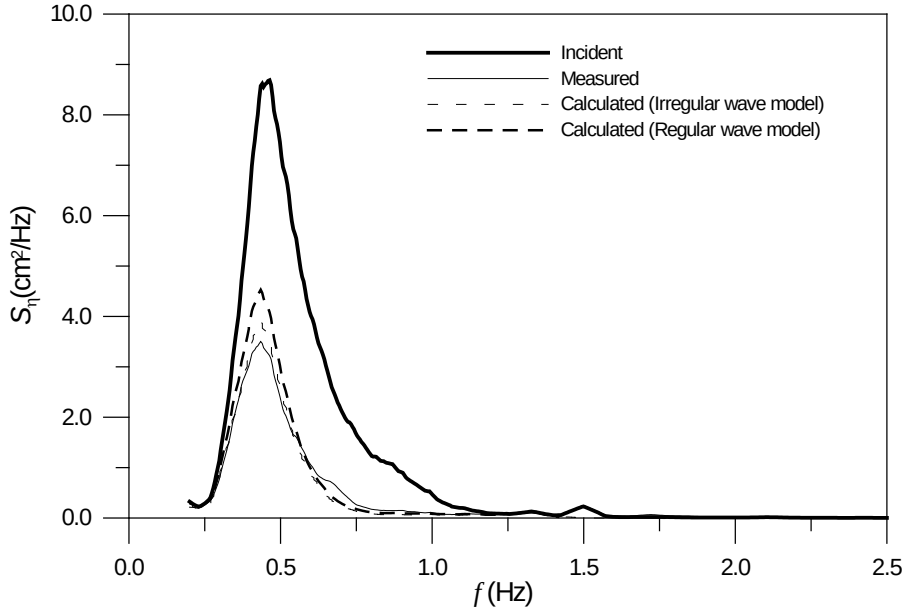

Fig. A.41. Measured and calculated spectra of incident and reflected waves ($H_s \cong 6$ cm, $T_s \cong 2.0$ s, $B = 45$ cm)

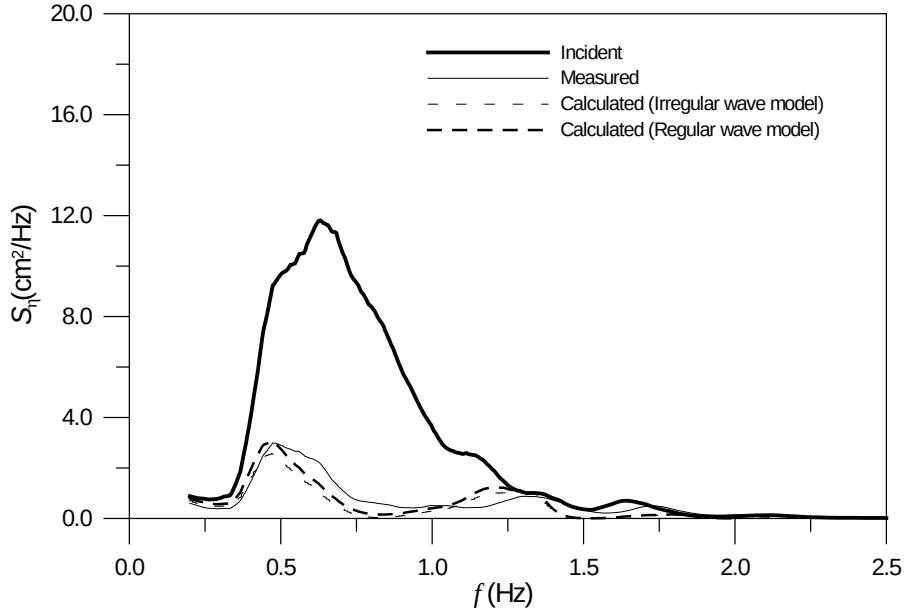

Fig. A.42. Measured and calculated spectra of incident and reflected waves ($H_s \cong 9$ cm, $T_s \cong 1.4$ s, $B = 45$ cm)

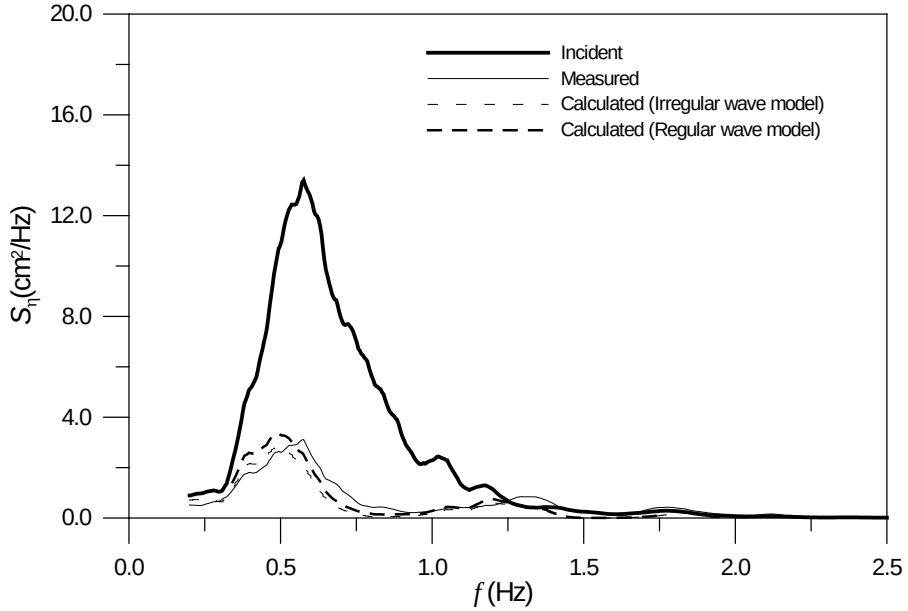

Fig. A.43. Measured and calculated spectra of incident and reflected waves ($H_s \cong 9$ cm, $T_s \cong 1.6$ s, B = 45 cm)

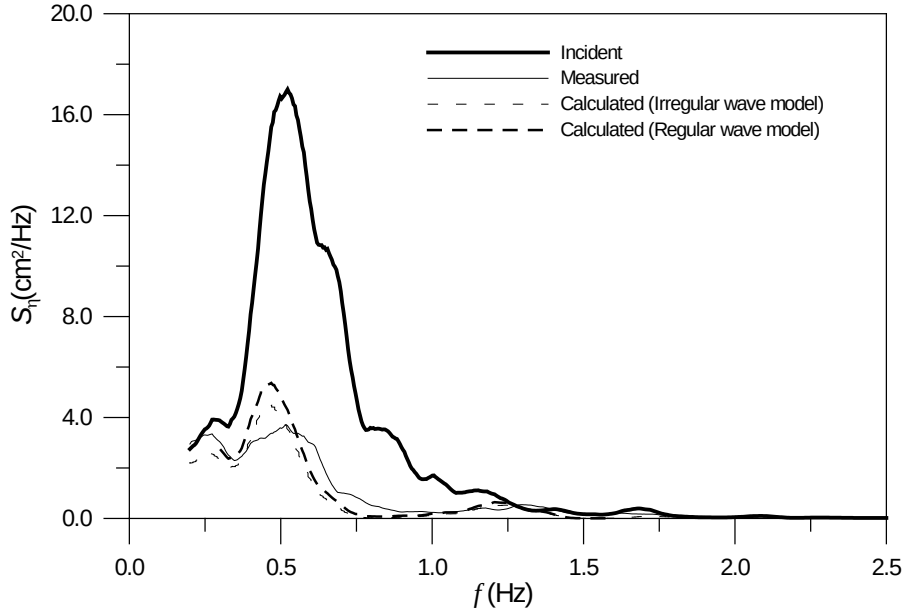

Fig. A.44. Measured and calculated spectra of incident and reflected waves ($H_s \cong 9$ cm, $T_s \cong 1.8$ s, B = 45 cm)

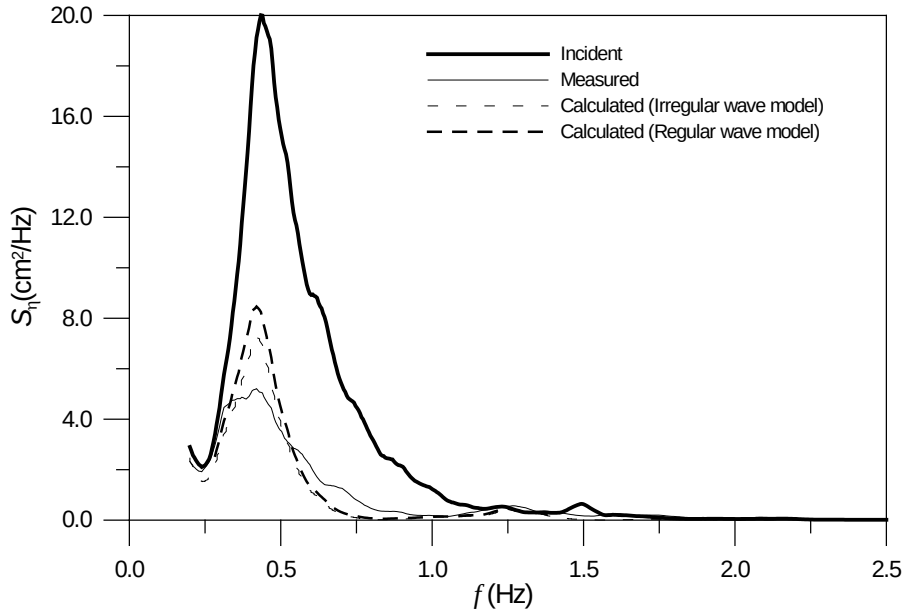

Fig. A.45. Measured and calculated spectra of incident and reflected waves ($H_s \cong 9$ cm, $T_s \cong 2.0$ s, $B = 45$ cm)

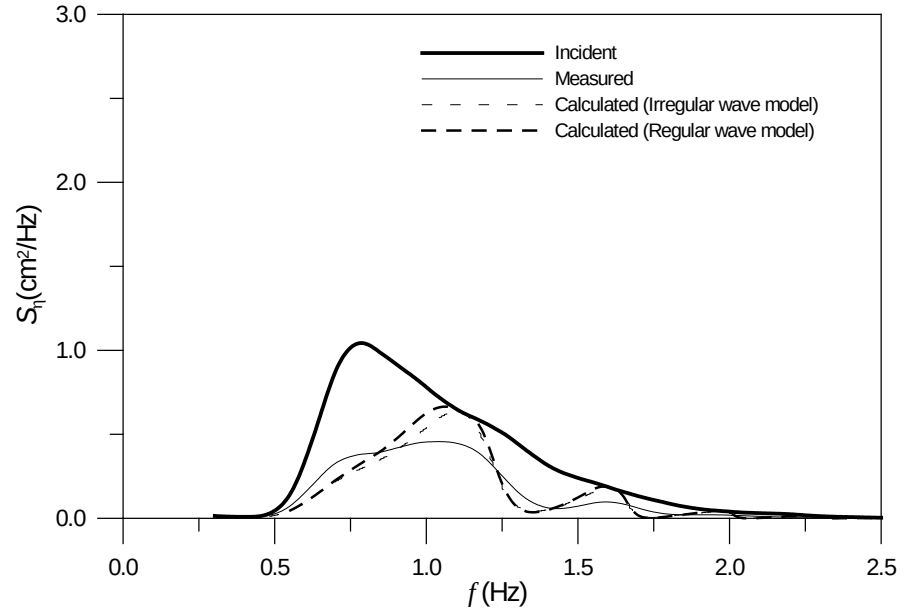

Fig. A.46. Measured and calculated spectra of incident and reflected waves ($H_s \cong 3$ cm, $T_s \cong 1.0$ s, $B = 60$ cm)

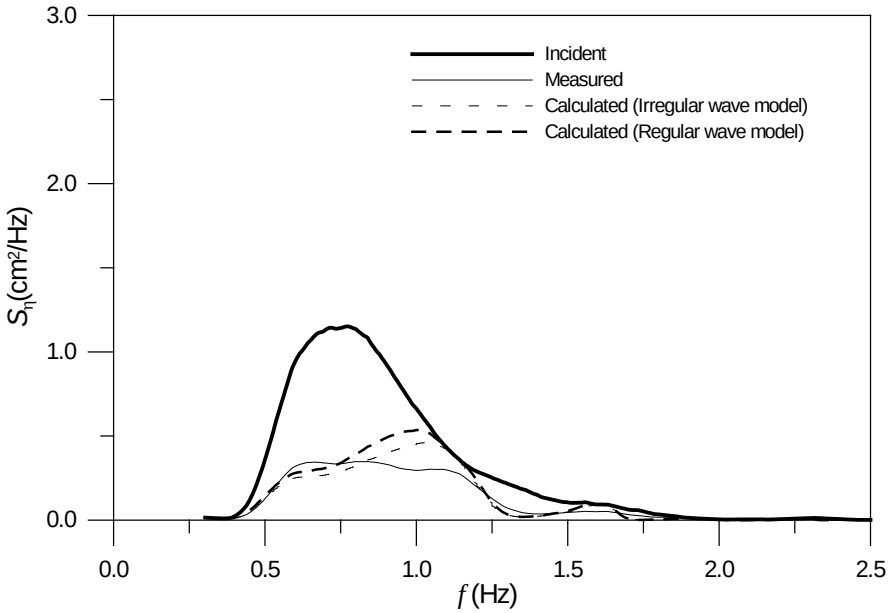

Fig. A.47. Measured and calculated spectra of incident and reflected waves ($H_s \cong 3$ cm, $T_s \cong 1.2$ s, B = 60 cm)

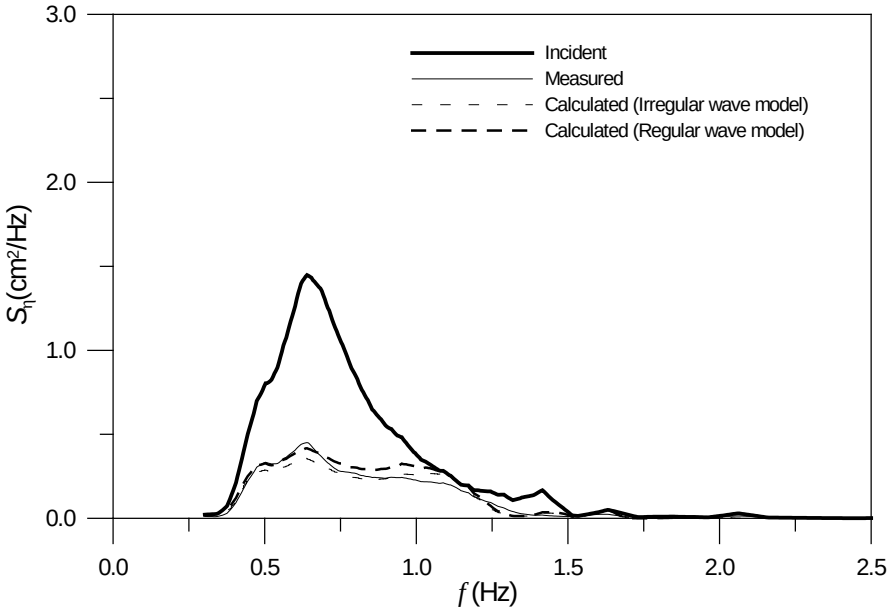

Fig. A.48. Measured and calculated spectra of incident and reflected waves ($H_s \cong 3$ cm, $T_s \cong 1.4$ s, B = 60 cm)

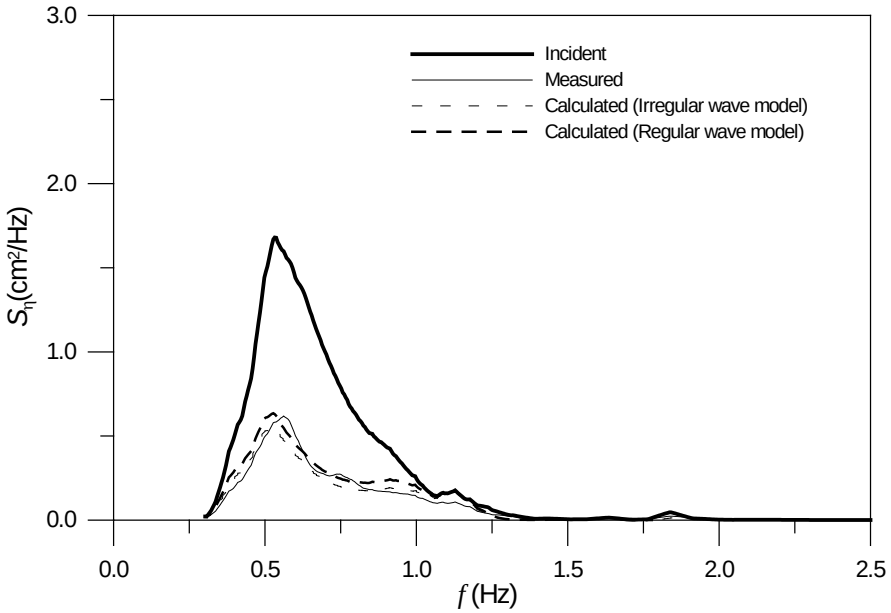

Fig. A.49. Measured and calculated spectra of incident and reflected waves ($H_s \cong 3$ cm, $T_s \cong 1.6$ s, B = 60 cm)

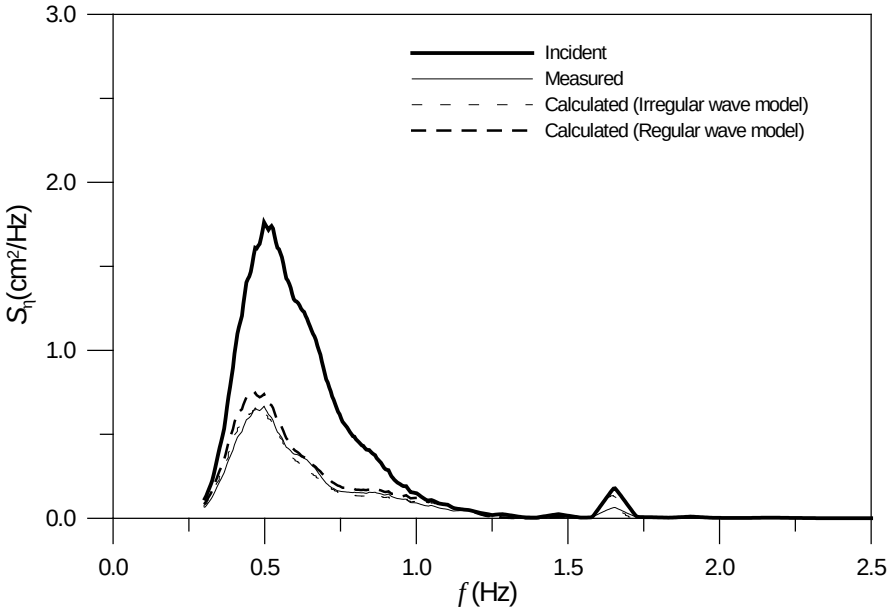

Fig. A.50. Measured and calculated spectra of incident and reflected waves ($H_s \cong 3$ cm, $T_s \cong 1.8$ s, B = 60 cm)

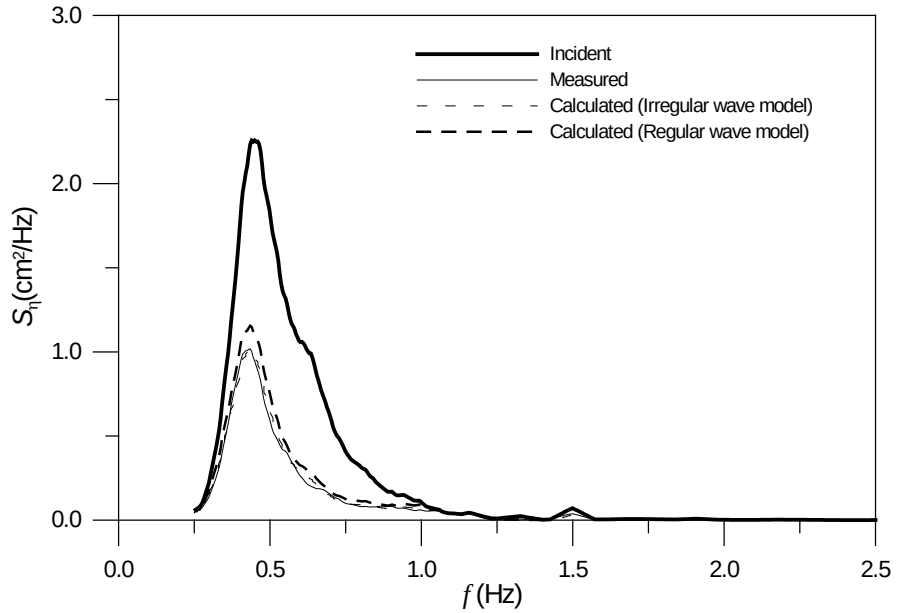

Fig. A.51. Measured and calculated spectra of incident and reflected waves ($H_s \cong 3$ cm, $T_s \cong 2.0$ s, $B = 60$ cm)

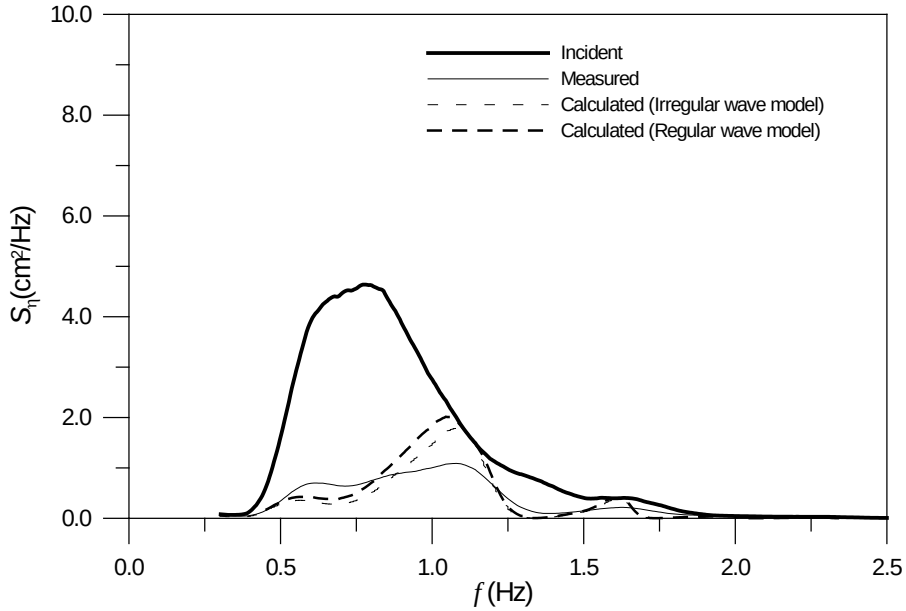

Fig. A.52. Measured and calculated spectra of incident and reflected waves ($H_s \cong 6$ cm, $T_s \cong 1.2$ s, $B = 60$ cm)

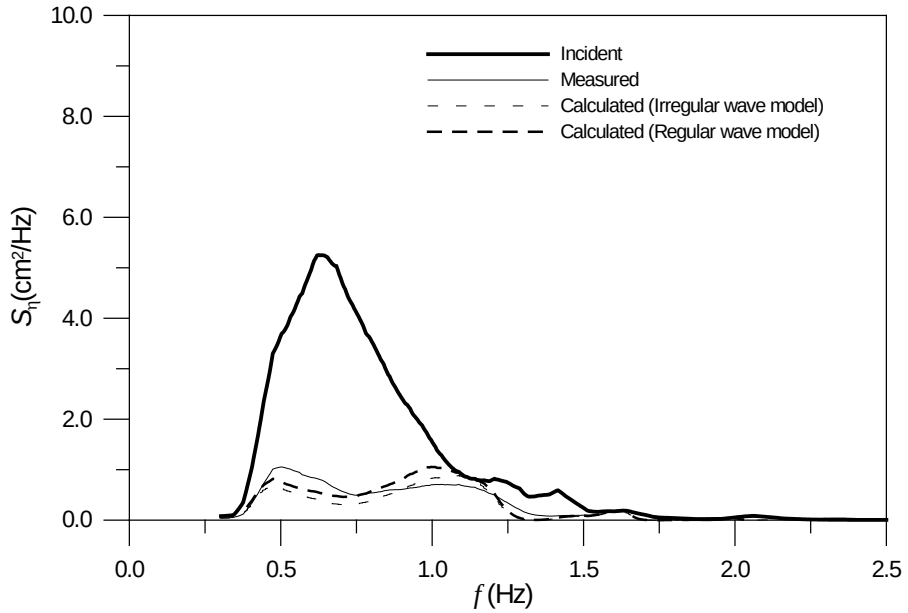

Fig. A.53. Measured and calculated spectra of incident and reflected waves ($H_s \cong 6$ cm, $T_s \cong 1.4$ s, $B = 60$ cm)

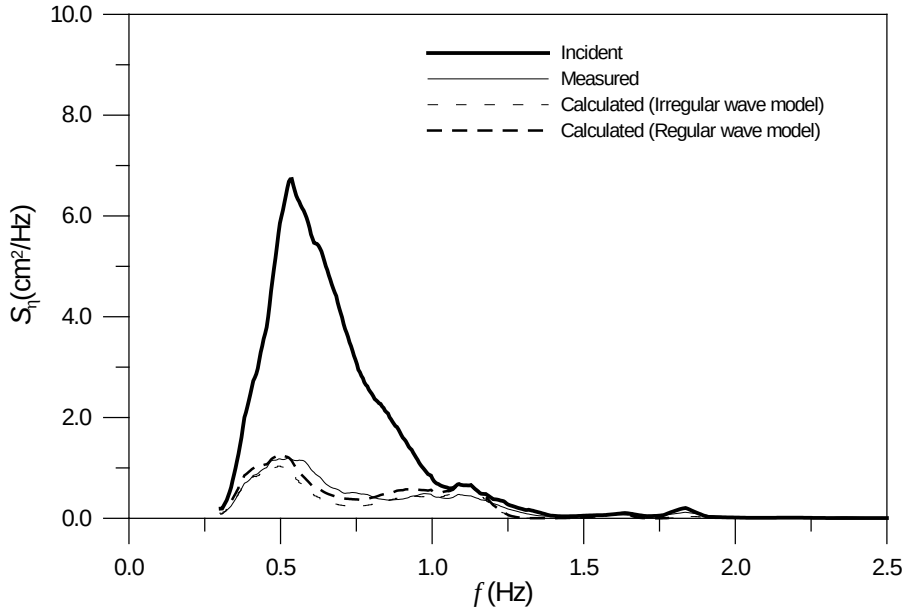

Fig. A.54. Measured and calculated spectra of incident and reflected waves ($H_s \cong 6$ cm, $T_s \cong 1.6$ s, $B = 60$ cm)

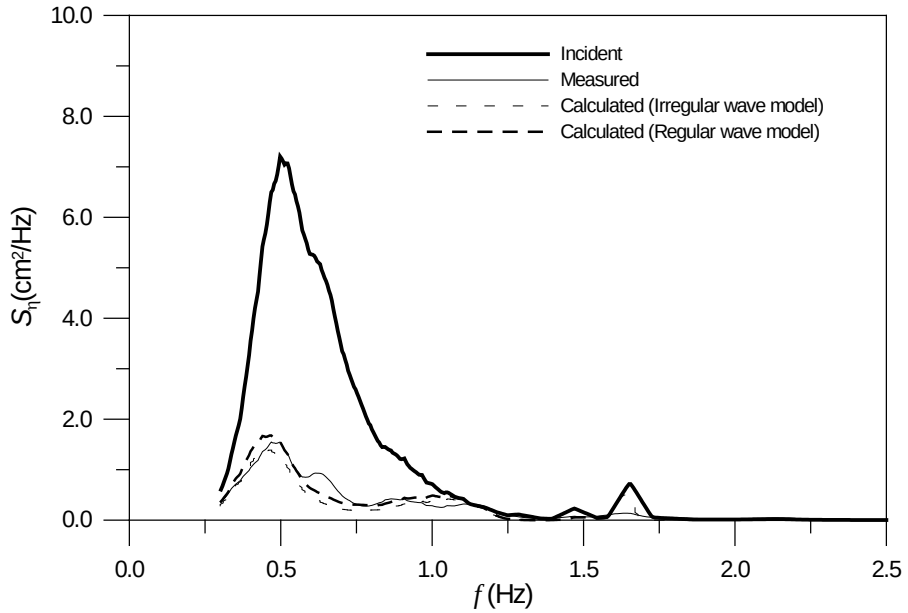

Fig. A.55. Measured and calculated spectra of incident and reflected waves ($H_s \cong 6$ cm, $T_s \cong 1.8$ s, $B = 60$ cm)

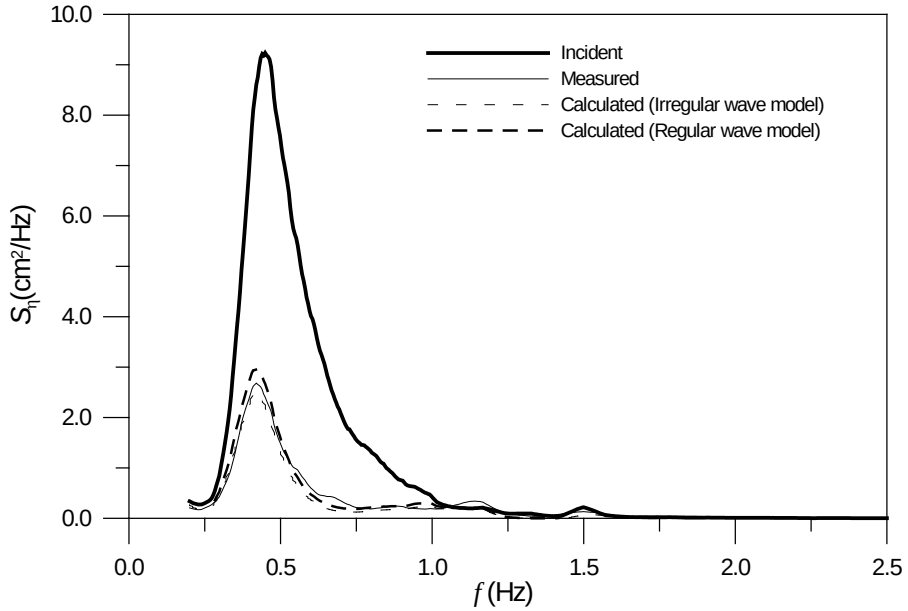

Fig. A.56. Measured and calculated spectra of incident and reflected waves ($H_s \cong 6$ cm, $T_s \cong 2.0$ s, $B = 60$ cm)

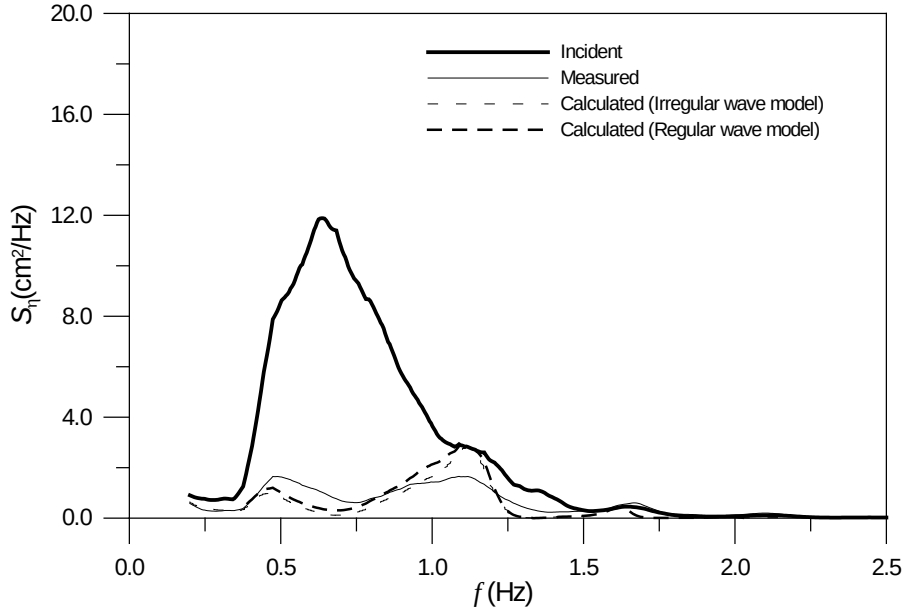

Fig. A.57. Measured and calculated spectra of incident and reflected waves ($H_s \cong 9$ cm, $T_s \cong 1.4$ s, B = 60 cm)

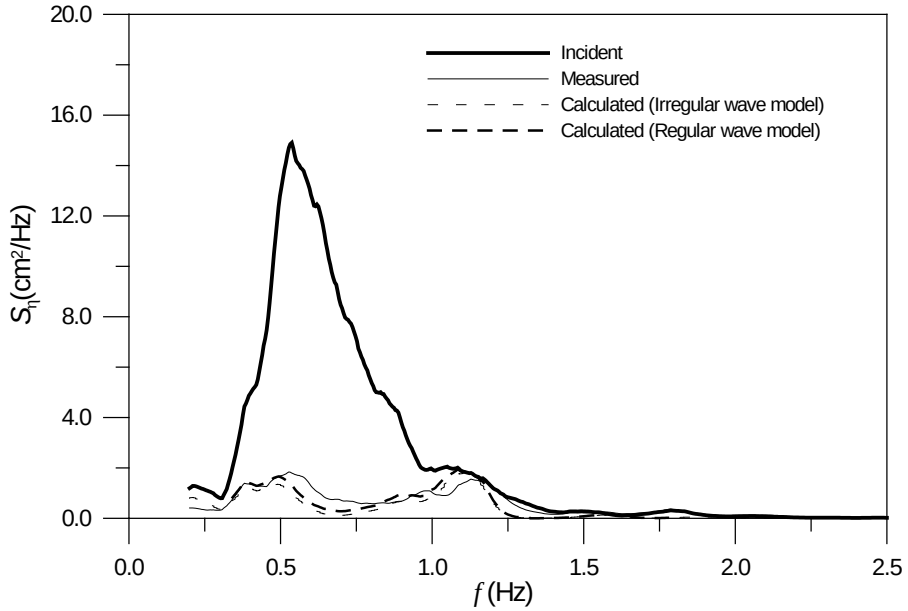

Fig. A.58. Measured and calculated spectra of incident and reflected waves ($H_s \cong 9$ cm, $T_s \cong 1.6$ s, B = 60 cm)

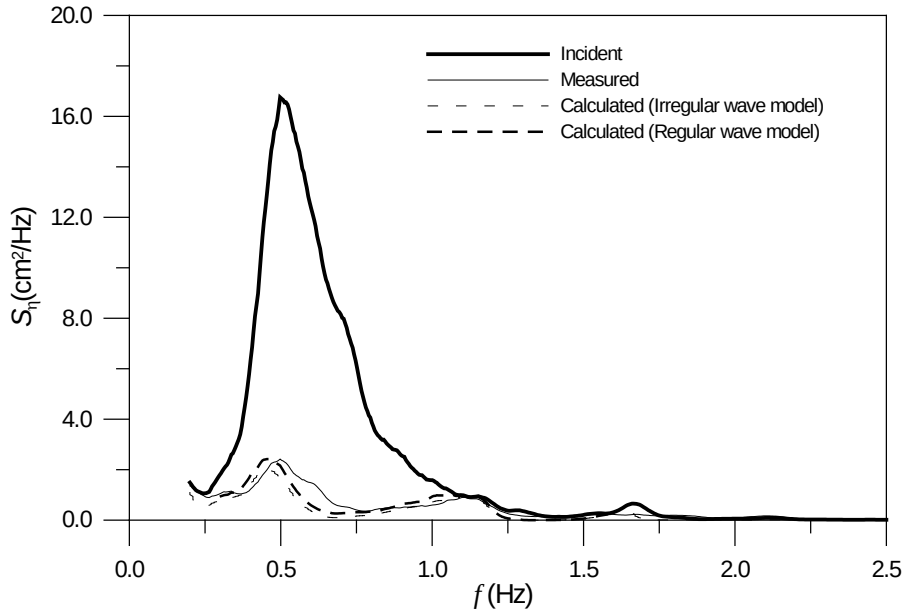

Fig. A.59. Measured and calculated spectra of incident and reflected waves ($H_s \cong 9$ cm, $T_s \cong 1.8$ s, B = 60 cm)

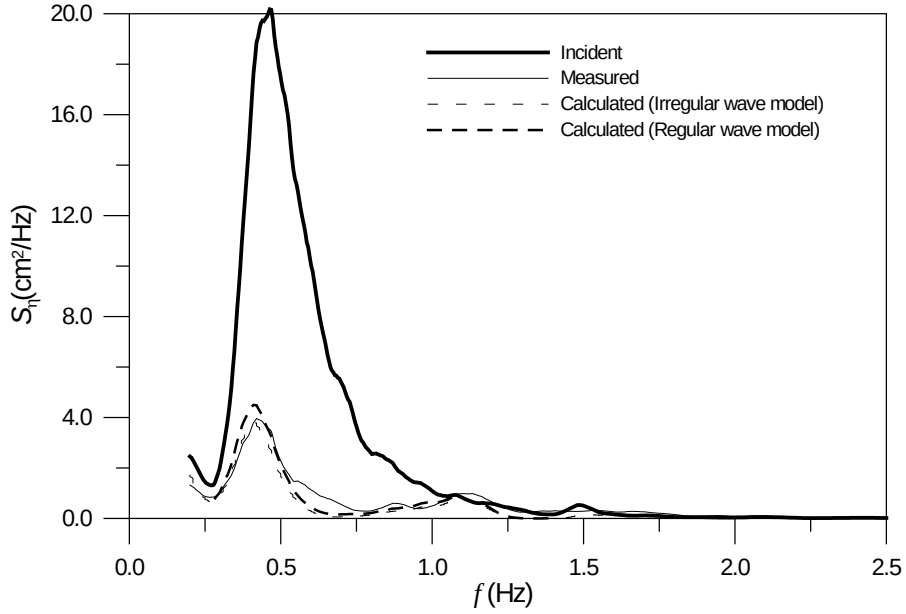

Fig. A.60. Measured and calculated spectra of incident and reflected waves ($H_s \cong 9$ cm, $T_s \cong 2.0$ s, B = 60 cm)

Appendix B. Photos of Laboratory Experiment

Photo 1. Wave flume at the Breakwater Laboratory of the Korea Institute Construction Technology

Photo 2. Perspective view of the wave flume

Photo 3. Longitudinal view of the wave flume

Photo 4. Wave scattering at the perforated wall

Photo 5. Wave gauges in the flume

초 록

규칙파 또는 불규칙파의 유공 케이슨 방파제로부터의 반사를 예측하는 해석모형은 이미 개발된 바 있다. 하지만 최근 Suh et al. (2001)에 의해 불규칙파 모델이 개발되었음에도 불구하고 여전히 규칙파 모델은 계산상의 단순성으로 인해 광범위하게 쓰인다. 본 연구에서는 Fugazza and Natale (1992)의 규칙파 모델을 이용하여 여러 가지 방법으로 유공 케이슨 방파제로부터의 불규칙파 반사율을 산정하였다.

우선 수리모형실험에 의해 규칙파 모델이 재 증명되었다. 반사율이 작을 때는 다소 과소 산정하는 반면 반사율이 클 경우에는 다소 과대 산정하였지만, 전반적으로 실험치와 계산치가 잘 일치했다.

이렇게 재확인된 규칙파 모델을 Suh et al. (2001)과 Bennett et al. (1992)의 불규칙파의 실험 결과에 적용하였다. 규칙파 모델을 불규칙파 반사율 산정에 적용함에 있어 몇 가지 방법이 이용되었는데, 결과적으로 모든 주파수대의 파고를 제곱평균의 제곱근한 파고라고 가정하고 규칙파 모델을 각 주파수대에 대해 반복적으로 사용하는 것이 가장 타당하였다.

주요어 : 규칙파, 불규칙파, 수리 실험, 파의 반사, 유공케이슨 방파제